LYMPHATICS

Lymph node stromal CCL2 limits antibody responses

Dragos C. Dasoveanu[1,2], Hyeung Ju Park[3], Catherine L. Ly[3], William D. Shipman[2,4,5], Susan Chyou[2]*, Varsha Kumar[2†], David Tarlinton[6], Burkhard Ludewig[7,8], Babak J. Mehrara[3], Theresa T. Lu[2,5,9,10‡]

Nonhematopoietic stromal cells in lymph nodes such as fibroblastic reticular cells (FRCs) can support the survival of plasmablasts and plasma cells [together, antibody-forming cells (AFCs)]. However, a regulatory function for the stromal compartment in AFC accumulation has not been appreciated. Here, we show that chemokine ligand 2 (CCL2)–expressing stromal cells limit AFC survival. FRCs express high levels of CCL2 in vessel-rich areas of the T cell zone and the medulla, where AFCs are located. FRC CCL2 is up-regulated during AFC accumulation, and we use lymph node transplantation to show that CCL2 deficiency in BP3$^+$ FRCs and lymphatic endothelial cells increases AFC survival without affecting B or germinal center cell numbers. Monocytes are key expressers of the CCL2 receptor CCR2, as monocyte depletion and transfer late in AFC responses increases and decreases AFC accumulation, respectively. Monocytes express reactive oxygen species (ROS) in an NADPH oxidase 2 (NOX2)–dependent manner, and NOX2-deficient monocytes fail to reduce AFC numbers. Stromal CCL2 modulates both monocyte accumulation and ROS production, and is regulated, in part, by manipulations that modulate vascular permeability. Together, our results reveal that the lymph node stromal compartment, by influencing monocyte accumulation and functional phenotype, has a regulatory role in AFC survival. Our results further suggest a role for inflammation-induced vascular activity in tuning the lymph node microenvironment. The understanding of stromal-mediated AFC regulation in vessel-rich environments could potentially be harnessed to control antibody-mediated autoimmunity.

INTRODUCTION

Lymphocytes in lymph nodes are supported by a nonhematopoietic stromal compartment composed of mesenchymal cells, blood vessels, and lymphatic sinuses. The mesenchymal cells, composed mainly of fibroblastic reticular cells (FRCs) that are marked by the expression of podoplanin (PDPN), ensheathe and produce the matrix components that make up a reticular network of collagen-rich fibrils (*1*–*3*). FRCs have additional functions in regulating immune cell positioning and lymphocyte survival and activity, and they interact closely with the blood vessels and lymphatic sinuses that transport oxygen, micronutrients, cells, and antigens to and from lymph nodes. During immune responses, the stromal compartment undergoes proliferative expansion and phenotypic alterations as lymph nodes grow (*4*, *5*). Fully understanding this dynamic compartment and how it shapes immune responses could aid in the development of stromal-focused approaches to modulate immunity in disease.

Plasmablasts and plasma cells [collectively referred to as antibody-forming cells (AFCs)] in secondary lymphoid organs are thought to contribute to autoantibody titers in diseases such as lupus (*6*–*8*). During T cell–dependent B cell responses, an initial burst of short-lived plasmablasts is followed by the accumulation of long-lived plasma cells (*9*, *10*). Plasmablasts in spleen are considered extrafollicular in origin, but in lymph nodes, they may also derive, in part, from germinal center responses. Both short- and long-lived cells are thought to migrate through the T cell zone (T zone) to accumulate in the medulla where most die and some, especially during secondary responses, will egress and home to the bone marrow to further mature and contribute to a long-lived pool (*9*–*12*).

Relatively little is known about the contributions of the lymph node microenvironment to regulating AFCs. We have shown that depletion of ZBTB46$^+$ dendritic cells (DCs) at day 8 after immunization with ovalbumin (OVA)–Alum leads to a 75% loss of AFCs at day 9 and that this was at least partly attributable to the loss of FRCs (*13*). The AFC loss was rescued by BAFF supplementation, suggesting that FRCs support AFCs by ligating BAFF-binding receptors on AFCs (*13*). Recently, T zone stromal cells bordering follicles were shown to express APRIL and BAFF that can promote AFC survival upon AFC exit from the germinal center (*14*). In addition, medullary FRCs support medullary cord AFCs via interleukin-6 (IL-6) production (*15*). Myeloid cells colocalize with AFCs as AFCs traverse the T zone to the medulla, and these myeloid cells express APRIL and IL-6 that could support AFCs (*12*). However, there is also evidence that at least some myeloid cells play regulatory roles. Depletion of LysM-Cre$^+$ or CCR2$^+$ cells at the initiation of, or early after immunization and deletion of, Myd88 or FcεR1γ in presumably myeloid cells increased AFC numbers (*16*–*18*). Similarly, CCR2 deficiency or monocyte depletion upon viral infection increased AFC numbers, and inducible nitric oxide synthase (iNOS) expressed by monocytes or monocyte-derived cells has been identified as one mediator (*17*, *19*). Together, studies suggest that FRCs promote AFC development and survival, whereas myeloid cells such as monocytes may play

[1]Physiology Biophysics and Systems Biology, Weill Cornell Graduate School of Medical Sciences, New York, NY 10065, USA. [2]Autoimmunity and Inflammation Program, Hospital for Special Surgery Research Institute, New York, NY 10021, USA. [3]Division of Plastic and Reconstructive Surgery, Department of Surgery, Memorial Sloan Kettering Cancer Center, New York, NY 10065, USA. [4]Weill Cornell/Rockefeller/Sloan-Kettering Tri-Institutional MD-PhD Program, New York, NY 10065, USA. [5]Immunology and Microbial Pathogenesis Program, Weill Cornell Graduate School of Medical Sciences, New York, NY 10065, USA. [6]Department of Immunology and Pathology, Monash University, Melbourne, Victoria 3004, Australia. [7]Institute of Immunobiology, Kantonsspital St. Gallen, St. Gallen CH-9007, Switzerland. [8]Institute of Experimental Immunology, University of Zürich, Zürich CH-8057, Switzerland. [9]Pediatric Rheumatology, Hospital for Special Surgery, New York, NY 10021, USA. [10]Department of Microbiology and Immunology, Weill Cornell Medicine, New York, NY 10065, USA.
*Present address: Viela Bio, Gaithersburg, MD, USA.
†Present address: Respiratory, Inflammation, and Autoimmunity Group, AstraZeneca, Gaithersburg, MD, USA.
‡Corresponding author. Email: lut@hss.edu

a regulatory role. Whether there is an FRC-AFC regulatory axis is unknown.

Here, we show that the stromal compartment, and especially FRCs, in AFC-rich areas in the T zone and medulla express high levels of chemokine ligand 2 (CCL2) and limit AFC survival. Monocytes are key CCL2-responsive cells that regulate AFCs in a manner dependent on NADPH (reduced form of nicotinamide adenine dinucleotide phosphate) oxidase 2 (NOX2), which is needed for reactive oxygen species (ROS) generation. We show that stromal CCL2 modulates both monocyte accumulation and ROS production and is regulated by manipulations that modulate vascular permeability. These results suggest a model whereby the lymph node stromal compartment, in addition to supporting AFCs, also functions to limit AFC responses and is, in part, regulated by the vasculature.

RESULTS

CCL2 is highly expressed by lymph node FRCs in the T zone and medulla

In examining for CCL2 expression, we analyzed CCL2 reporter mice produced by bacterial artificial chromosome (BAC)–mediated transgenesis that express CCL2 linked to green fluorescent protein (GFP). The GFP is clipped off in the cytosol and remains there to mark CCL2-producing cells ["M1R" mice from (*20*)]. In homeostatic lymph nodes, GFP was expressed in the T zone and medulla and excluded from B cell follicles (Fig. 1A). Within the T zone, vascular-rich regions under the follicles known as the cortical ridge (*21*) and vascular cords running toward the medulla (*22*) are recognizable by the high density of ER-TR7$^+$ vessels, and GFP was most brightly expressed in these areas (Fig. 1A). Bone marrow chimeras repopulating CCL2-GFP hosts with wild-type (WT) bone marrow (WT→CCL2-GFP chimeras) showed a similar pattern of GFP expression (Fig. 1B), suggesting that CCL2^{hi}-expressing cells in the T zone and medulla could be stromal in origin. Consistent with this idea, GFP was mostly expressed in a reticular pattern (Fig. 1C), although round, likely hematopoietic, GFP-expressing cells were also seen (Fig. 1C, arrowheads). Flow cytometric analysis confirmed that both CD45$^+$ hematopoietic and CD45$^-$ nonhematopoietic cells expressed GFP (Fig. 1D). CD45$^+$ GFP$^+$ cells were mostly CD11b$^+$ myeloid cells and could be divided into Ly6C$^+$ presumed monocytes and Ly6C$^-$ cells (Fig. 1D). The majority of CD45$^-$ GFP$^+$ cells were CD31$^-$PDPN$^+$ FRCs, and under 20% were CD31$^+$PDPN$^+$ lymphatic endothelial cells (LECs) (Fig. 1D). FRCs expressed the highest level of GFP when compared with LECs and CD11b$^+$ cells (Fig. 1E). Together, these results suggested that FRCs are major CCL2 expressers in homeostatic lymph nodes, with LECs and myeloid cells expressing lower levels of CCL2.

We further examined the characteristics of the GFP-expressing FRCs. BP3/CD157/BST-1 marks well-differentiated CCL21-expressing T zone FRCs (fig. S1A) as well as CXCL13-expressing marginal reticular cells (MRCs) and follicular dendritic cells (FDCs) (*21*, *23*, *24*). Consistent with recent findings (*15*), the medulla is generally dimmer for BP3, although stromal BP3 staining is detectable within medullary cords in both homeostatic and immunized lymph nodes (fig. S1B). (PDPN$^+$) BP3$^{lo\text{-}neg}$ cells are composed mainly of CD34$^+$ reticular cells that are also Sca1$^+$ (fig. S1A), and have been shown to be perivascular and have progenitor potential (*25*, *26*). GFP was expressed at higher levels by BP3$^+$ cells than by BP3$^{lo\text{-}neg}$ cells in CCL2-GFP mice (Fig. 1F), as was intracellular CCL2 protein (fig. S1C). The BP3$^+$ CCL2^{hi} expressers were also found in the CCL21$^+$ population (Fig. 1G), supporting the idea that the high CCL2 expression in the cortical ridge and paracortical vascular cords was by T zone FRCs. Together, these results indicated that CCL2 is expressed most highly by BP3$^+$ FRCs, some of which are T zone FRCs.

Stromal CCL2 is up-regulated with immunization and colocalizes with AFCs

The regions of high stromal CCL2 are also areas of AFC accumulation (*12*, *14*), leading us to ask whether stromal CCL2 regulated AFCs. A kinetic analysis of B cell responses in popliteal lymph nodes after OVA-Alum immunization showed that germinal center B cells and immunoglobulin G$^+$ (IgG$^+$) AFCs were detectable in large numbers by day 9 (fig. S2, A and B). The AFCs showed a high proliferative rate at day 9, suggesting that many were plasmablasts (fig. S2C). By day 12, AFC numbers had dropped (fig. S2, A and B), consistent with the apoptosis of plasmablasts seen in spleen (*10*, *27*) and the drop seen in lymph nodes (*11*, *12*), and remained at day 12 levels at least through day 15 (fig. S2, A and B). At days 12 to 15, the AFC proliferation rate was lower than at day 9 but still at about 12% (fig. S2C), suggesting that the steady AFC numbers between days 12 and 15 reflected continuous cell turnover, with a balance mainly between proliferation and apoptosis. Because this day 12 to 15 window allowed for investigation of AFC proliferation and survival, we focused our efforts on studying this time period.

To assess the role of stromal CCL2 in regulating AFCs, we examined for immunization-induced alterations in CCL2 expression in reporter mice and colocalization of AFCs and CCL2 in WT→CCL2-GFP chimeras. BP3$^+$ FRCs up-regulated GFP expression by day 9 after immunization (Fig. 2A), as did CCL21$^+$ FRCs (Fig. 2, A and B), suggesting that T zone FRCs were among the cells that up-regulated CCL2. CCL21$^-$ FRCs, some of which are medullary and/or interfollicular cells (*26*, *28*, *29*), showed an early up-regulation of CCL2 at day 2, which decreased by day 15 (Fig. 2B). LECs, but not myeloid cells, also showed CCL2 up-regulation after immunization, although LEC CCL2 expression remained quite low compared with that of FRCs and had returned to nearly homeostatic levels by day 15 (Fig. 2, A and B). At both days 10 and 15 after OVA-Alum immunization, CCL2 expression was highest in regions of AFC localization (Fig. 2C and fig. S2D). The colocalization of CCL2-expressing FRCs with AFCs suggested a potential functional interaction between the two.

Lymph node stromal CCL2 regulates AFC numbers and survival

We examined the effect of CCL2 deficiency on AFC responses. Although B cell numbers were similar in homeostatic WT and *Ccl2*$^{-/-}$ mice (fig. S3A), *Ccl2*$^{-/-}$ mice at day 15 after OVA-Alum showed increased numbers of total B cells, germinal center B cells, and AFCs with no change in T cell numbers (Fig. 3A). The increased AFCs in CCL2-deficient mice were accompanied by increased anti-OVA–secreting cells and anti-OVA serum IgG (Fig. 3, B and C). Because the increase in AFCs in *Ccl2*$^{-/-}$ mice could be a consequence of increased germinal center B cell numbers, we further characterized the AFCs. AFCs in *Ccl2*$^{-/-}$ mice showed no change in ki67 expression but had decreased activated caspase-3 levels (Fig. 3, D and E), suggesting that they were proliferating at similar rates but undergoing less apoptosis than WT AFCs. Anti-OVA–secreting cell numbers in bone marrow were similar (Fig. 3F), suggesting that the increased lymph node AFC accumulation was not because of reduced emigration from lymph node to bone marrow. AFCs localized to

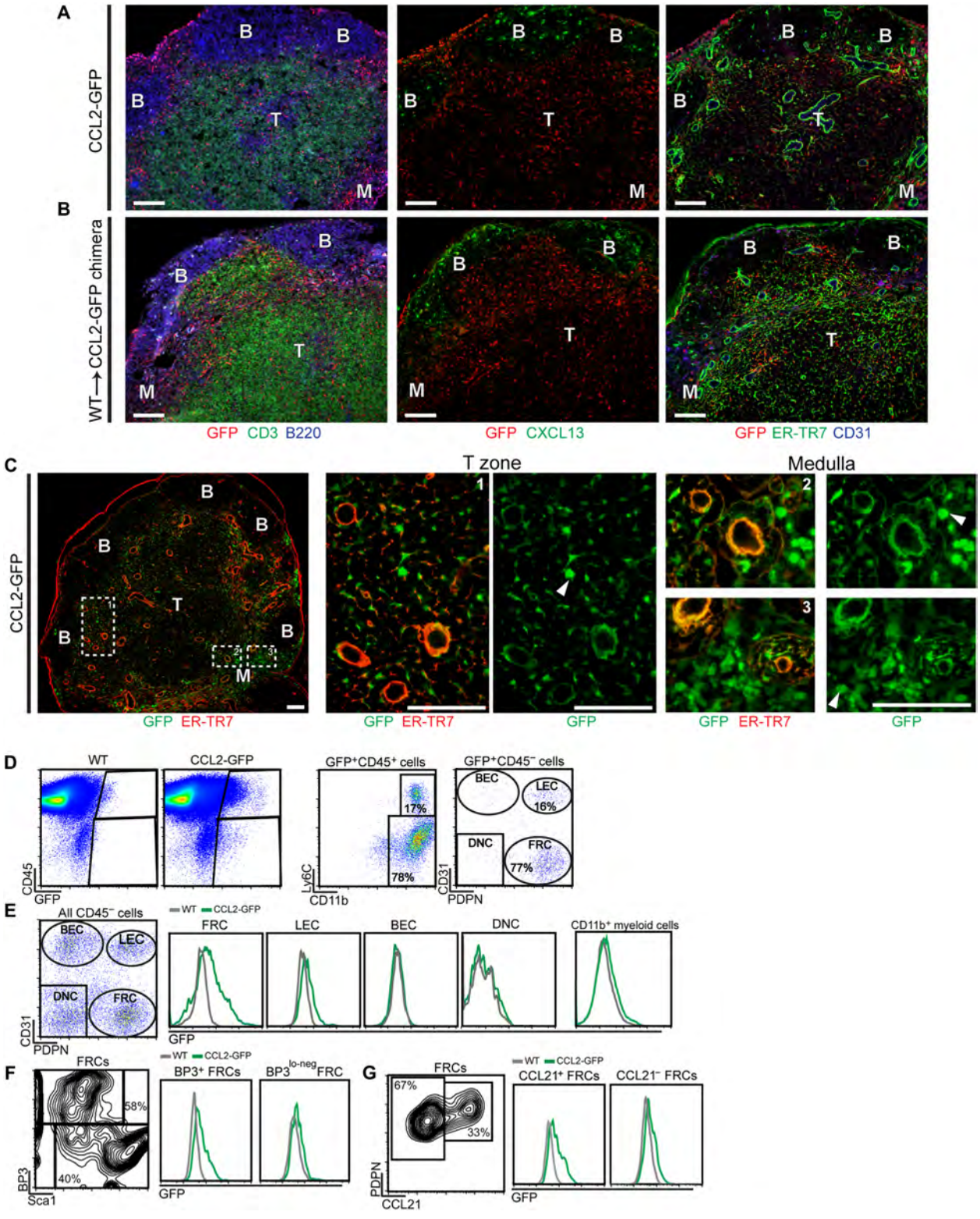

Fig. 1. Lymph node stromal cells in the T zone and medulla express CCL2. (**A** to **G**) Homeostatic brachial lymph nodes from indicated mice were examined. (A and B) Sections from (A) CCL2-GFP mice and (B) WT→CCL2-GFP chimeras were stained for GFP and indicated markers. B, B cell follicles; T, T zone; M, medulla. (C) Magnified views of GFP-expressing cells. Arrowheads point to round cells. (D to G) Flow cytometric characterization of cells from CCL2-GFP mice. Fluorescence scale is $\log_{10}$. (D) Characterization of GFP$^+$ cells. BEC, blood endothelial cells; FRC, fibroblastic reticular cells; DNC, double-negative cells. (E) Histograms depicting GFP levels in indicated cell populations. (F and G) Density plots and histograms showing GFP expression in indicated FRC subsets. (A to C) Scale bars, 100 μm. (A to G) Results are representative of $n \geq 3$ mice per condition.

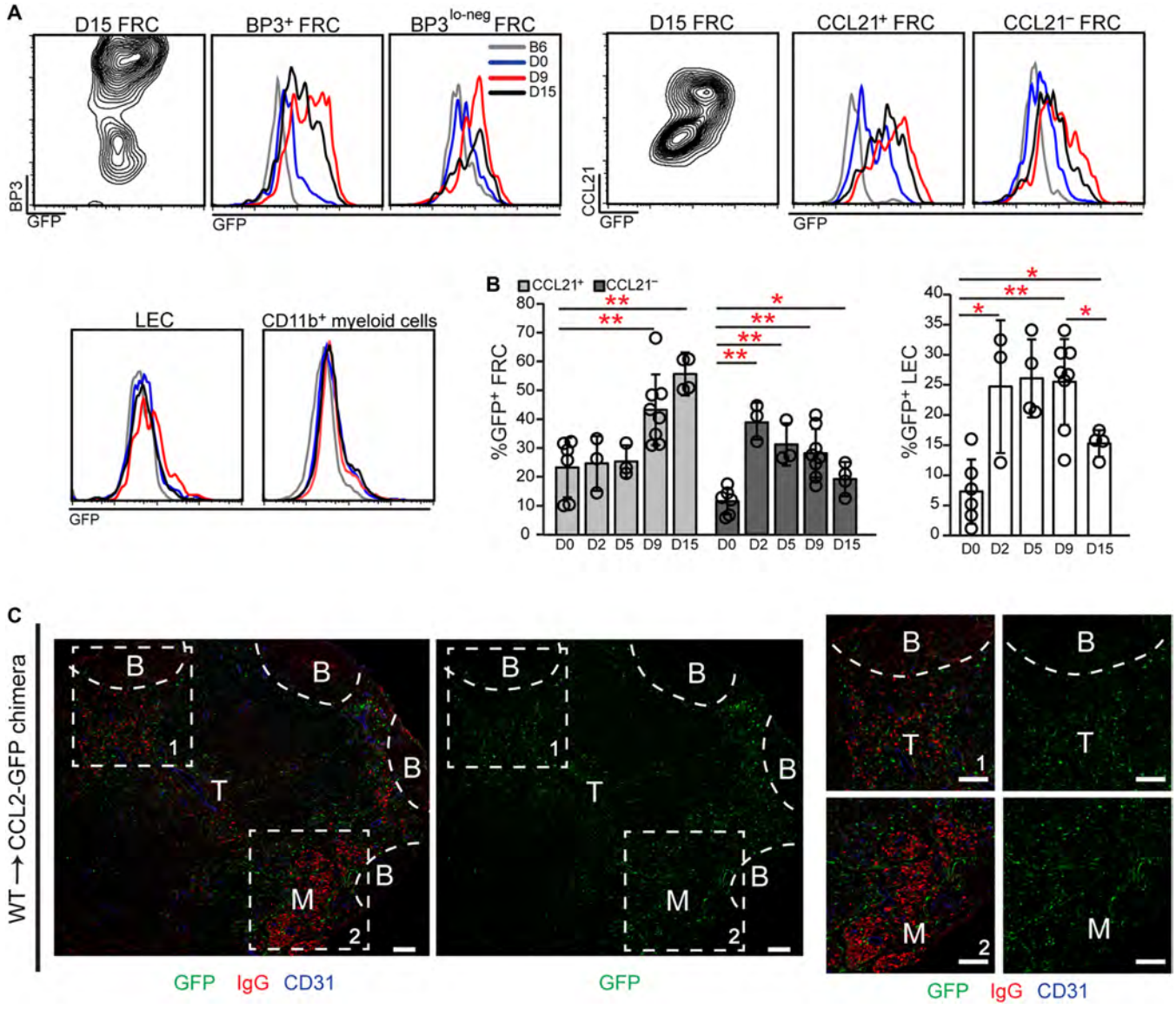

Fig. 2. Stromal CCL2 is up-regulated upon immunization and colocalizes with AFCs. (**A** to **C**) CCL2-GFP mice or WT→CCL2-GFP chimeras were immunized in footpads with OVA-Alum on day 0 (D0), and popliteal nodes were harvested on indicated days. (A) Contour plots and histograms show GFP levels in the indicated cells. Fluorescence scale is $\log_{10}$. (B) Percentage of FRCs and LECs that are GFP$^+$ over time. Each symbol represents one mouse; $n = 3$ to 8 per condition over five experiments. *$P < 0.05$, **$P < 0.01$ using two-tailed unpaired Student's t test. Error bars represent SD. (C) GFP and AFC localization. Sections from day 15 WT→CCL2-GFP chimeras were stained for GFP, mouse IgG, and CD31. Representative of $n \geq 3$ mice. Scale bars, 100 μm.

the T zone and medulla in both WT and *Ccl2*$^{-/-}$ lymph nodes (Fig. 3G). These data suggested that CCL2 limits B cell responses and AFC survival.

We further assessed the role of CCL2 on a germinal center–independent lymph node AFC response and on splenic responses. At 8 days after footpad lipopolysaccharide (LPS) immunization, *Ccl2*$^{-/-}$ lymph nodes showed unchanged T and B cells, an almost twofold increase in AFC numbers (Fig. 3H), and reduced AFC activated caspase-3 (Fig. 3I). However, splenic responses to OVA-Alum and NP-Ficoll were similar in WT and *Ccl2*$^{-/-}$ mice (fig. S3, B and C). These results suggested that CCL2 can regulate lymph node AFC survival independent of an effect on germinal centers and that CCL2 does not play the same role in splenic responses in our models.

We asked about the role of stromal-derived CCL2. We considered crossing the *Ccl19*-Cre driver (*30*) with *Ccl2*$^{f/f}$ mice (*20*) to delete FRC CCL2. However, *Ccl19*-Cre;YFP$^{f/STOP/f}$ mice showed that only 52% of BP3$^+$ FRCs (±12%; $n = 3$ mice) were YFP$^+$ and BP3$^{lo\text{-}neg}$ FRCs expressed very little yellow fluorescent protein (YFP) at day 15 after immunization (fig. S4), suggesting that FRC CCL2 would not be fully deleted in our model. We thus used a lymph node transplant model (*31*) where we transplanted (CD45.2) WT and *Ccl2*$^{-/-}$ popliteal lymph nodes into CD45.1 mice (Fig. 4, A and B). In similar systems, transplanted lymph node tissue is repopulated by recipient hematopoietic cells, whereas the stromal compartment remains donor derived (*32*, *33*). Although we initially performed bilateral transplantations (Fig. 4A), recovery rate of transplanted lymph nodes was only

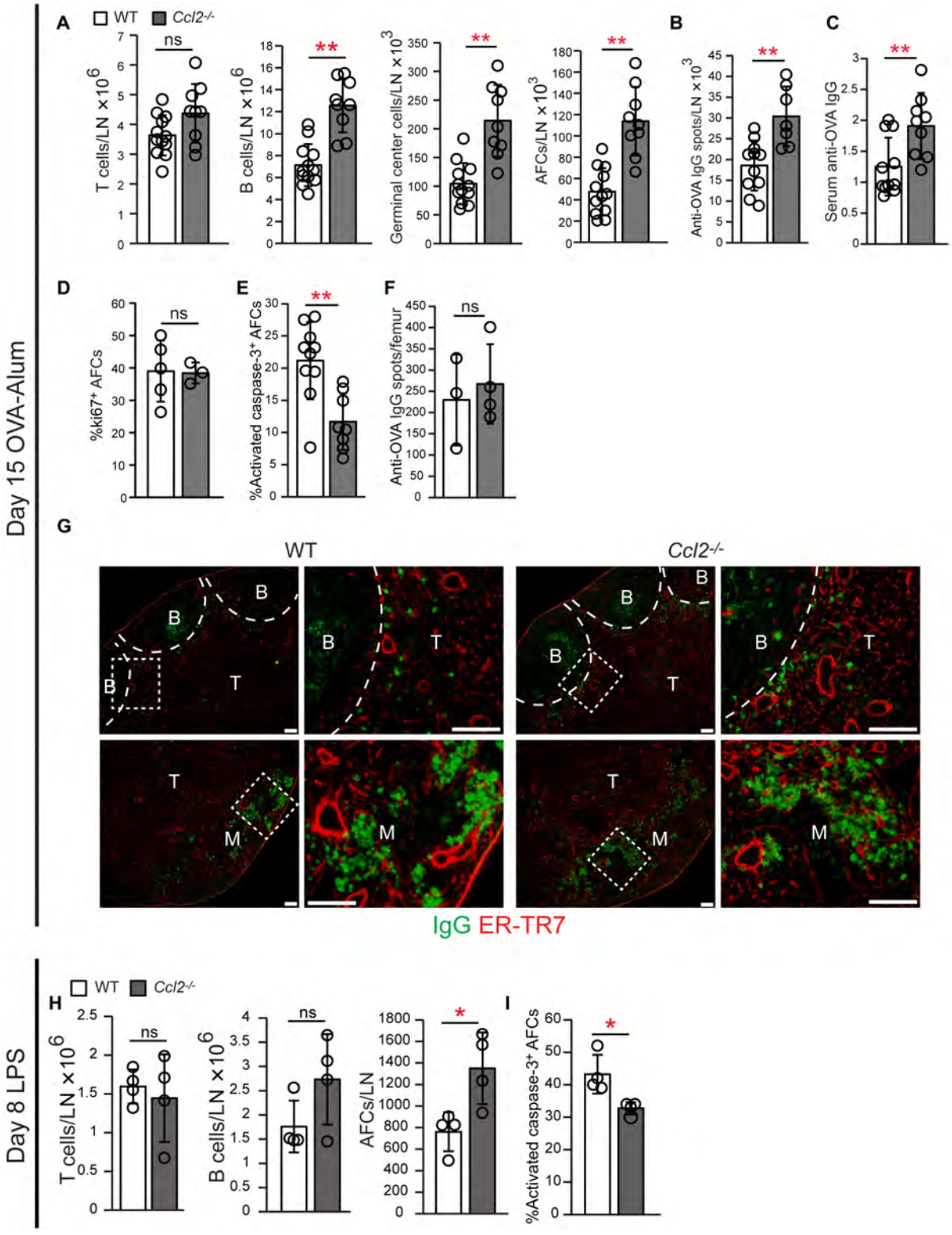

Fig. 3. *Ccl2*$^{-/-}$ mice show increased AFC accumulation and survival. (**A** to **G**) WT and *Ccl2*$^{-/-}$ mice were immunized on day 0 and examined on day 15. (A) Numbers of indicated cell type/lymph node (LN) by flow cytometric analysis. (B) Anti-OVA IgG spots/lymph node using ELISpot. (C) Anti-OVA IgG serum titers. (D and E) Percentages of lymph node AFCs positive for (D) ki67 and (E) activated caspase-3. (F) Anti-OVA IgG spots in bone marrow using ELISpot. (G) Representative lymph node sections stained for mouse IgG and ER-TR7. Scale bars, 100 μm. (**H** and **I**) WT and *Ccl2*$^{-/-}$ mice were injected with LPS in footpads on day 0 and examined on day 8. (A to F, H, and I) Each symbol represents one mouse; $n = 3$ to 12 per condition; data are from five to six (A to C and E) and two (D, F, H, and I) experiments. $^{**}P < 0.01$ by two-tailed unpaired Student's *t* test. Error bars represent SD. ns, not significant.

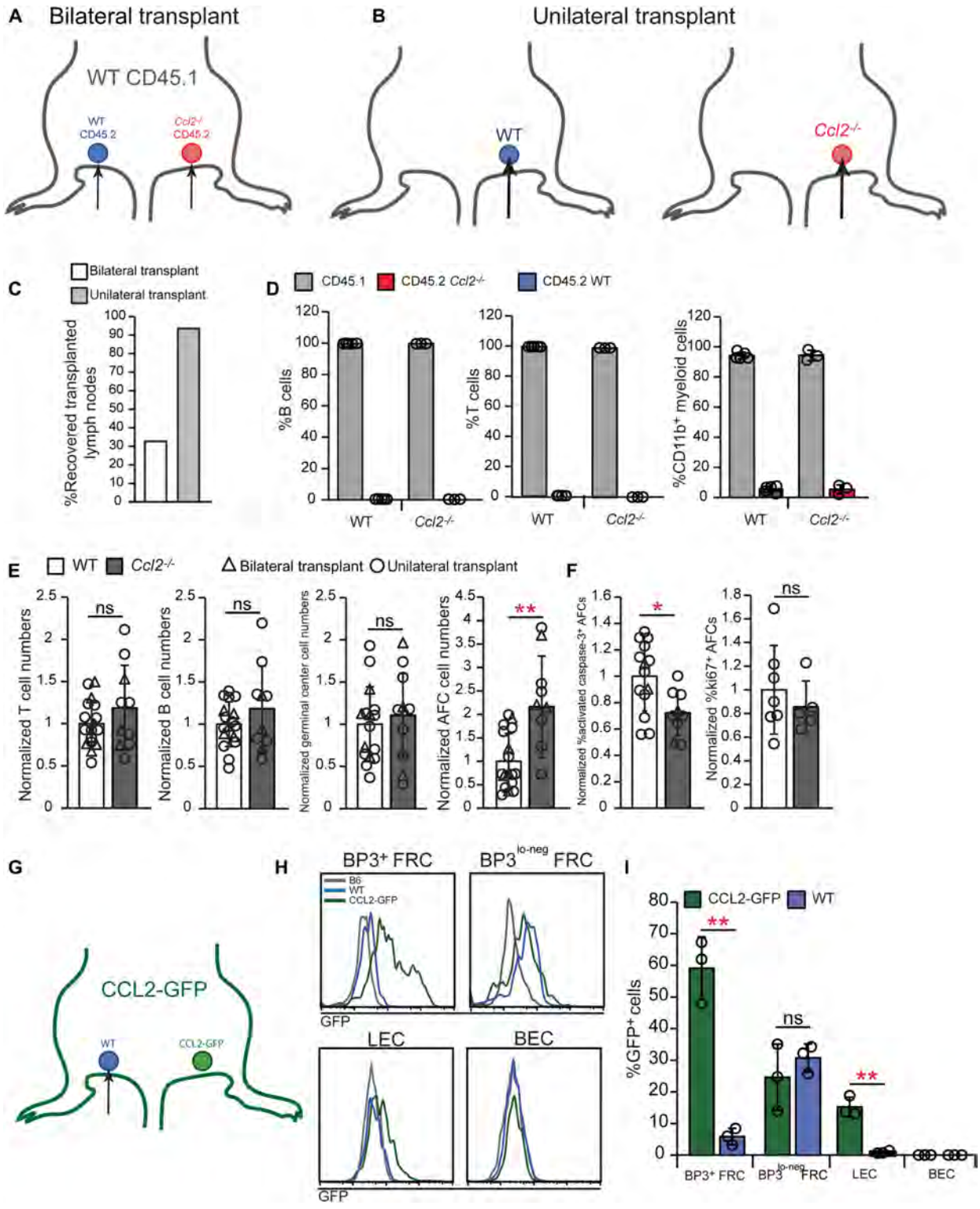

Fig. 4. Lymph node stromal CCL2 limits AFC survival. (**A** to **F**) WT CD45.1$^+$ hosts received either bilateral (A) or unilateral (B) lymph node transplants, as indicated, before immunization with OVA/Alum and examination 15 days later. (C) Recovery rate of bilateral or unilateral transplanted lymph nodes. (D) Percentages of B, T, and CD11b$^+$ cells that were host (CD45.1$^+$) and donor (CD45.2$^+$) derived. Data are from bilateral transplants. (E) Normalized numbers of indicated cells/lymph node. (F) Normalized percentage of AFCs that are activated caspase-3$^+$ or ki67$^+$. (**G** to **I**) WT nodes were transplanted into left side of CCL2-GFP mice, as depicted in (G). (H) Histograms showing GFP expression in indicated cells from WT donor or CCL2-GFP host lymph nodes. "B6" node is from an untransplanted WT mouse. Fluorescence scale is $\log_{10}$. (I) Percentages of indicated cells that are GFP$^+$. (D to F and I) Each symbol represents one lymph node; $n = 3$ to 17 mice per condition from 2 (D), 11 (3 bilateral, 8 unilateral transplants) (E and F), and 1 (I) independent experiments. *$P < 0.05$, **$P < 0.01$ by two-tailed unpaired Student's t test. Error bars represent SD.

32% (Fig. 4C), leading us to perform unilateral transplantations (Fig. 4B). Unilateral transplantations improved lymph node recovery to 93% (Fig. 4C), and the results of unilateral and bilateral transplantations were pooled as indicated.

As early as 4 weeks after transplantation, recovered homeostatic lymph nodes showed normal organization, with robust B cell follicles, FDCs, and reticular pattern of ER-TR7 staining in the T zone (fig. S5A). After immunization, germinal centers and AFCs, when they were seen in sections, appeared normal in location (fig. S5B). The T, B, and myeloid cells in the transplanted lymph nodes were almost entirely CD45.1$^+$ (i.e., recipient derived), as expected (Fig. 4D).

Of the recovered lymph nodes, we further examined for optimal and suboptimal transplants. Lymph node B cell numbers increase disproportionately relative to T cell numbers upon immunization (fig. S6A) (*34*, *35*), but we found that some transplanted immunized lymph nodes had an abnormally low B:T cell ratio of less than 1 (fig. S6A). This phenotype suggested that the signals from the immunized footpad did not reach the transplanted lymph node and likely reflected incomplete reconstitution of the vascular connections, and we termed these lymph nodes as "suboptimal transplants." The low B:T cell ratio occurred in both unilateral and bilateral transplants (fig. S6B) and in both WT and *Ccl2*$^{-/-}$ genotypes, consistent with the idea that this phenotype reflected poor transplant quality (fig. S6C). We excluded these suboptimal transplants from further analysis.

Relative to the WT controls, immunized transplanted *Ccl2*$^{-/-}$ lymph nodes showed no difference in the numbers of total, T, B, or germinal center B cells. AFCs, however, showed increased numbers, decreased activated caspase-3 expression, and no change in proliferation (Fig. 4, E and F, and fig. S6, D to G). These AFC-specific effects pointed to a key role for the lymph node stromal compartment and its expression of CCL2 in limiting AFC survival.

To assess the degree to which different FRC subpopulations in our system were donor derived, we transplanted WT popliteal lymph nodes into one side of CCL2-GFP reporter mice (Fig. 4G) and assessed for recipient GFP$^+$ FRCs in the (GFP$^-$) donor lymph nodes. In transplanted WT lymph nodes, BP3$^+$ FRCs showed very low levels of GFP, whereas BP3$^{lo\text{-}neg}$ FRCs were comparable in GFP expression with native (CCL2-GFP) lymph node BP3$^{lo\text{-}neg}$ FRCs (Fig. 4, H and I). These results suggested that, in transplanted nodes, the CCL2 ^{hi}-expressing BP3$^+$ FRCs remain largely donor derived, whereas the CCL2^{lo}-expressing BP3$^{lo\text{-}neg}$ FRCs are replaced by host cells. In addition, transplanted lymph node LECs did not show GFP expression, suggesting that they remain entirely donor derived (Fig. 4, H and I). In summary, the transplanted lymph nodes retain BP3$^+$ FRCs and LECs but not BP3$^{lo\text{-}neg}$ FRCs. Our results together supported a role for CCL2 expressed by lymph node BP3^{hi} FRCs and/or LECs in regulating AFC accumulation and survival.

Monocytes are key CCR2$^+$ cells that regulate AFC survival late in immune responses

CCL2 interacts with CCR2 (*36*), and we sought to identify CCR2$^+$ cells that regulated AFC survival in our system. We did not observe CCR2 expression by AFCs using either *Ccr2*-GFP mice (*37*) or CCR2 antibody staining (fig. S7A), suggesting that lymph node stromal CCL2 regulated AFCs indirectly. GFP was expressed mostly by CD11b$^+$ myeloid cells, the majority of which consisted of Ly6C^{hi} presumed monocytes (*38*, *39*) and Ly6C^{lo} cells (Fig. 5A). The Ly6C^{lo} cells were composed of (i) MHCII^{hi}EpCAM$^-$CD103$^-$ cells (Fig. 5A) that were CCR7$^+$ (fig. S7B), consistent with their identity as dermal or monocyte-derived DCs that migrated from skin (*39*), and (ii) CD11c^{hi} CD8$^-$ cells that could be resident DCs or monocyte-derived cells (*40*, *41*). Ly6C^{hi} cells uniformly expressed GFP (Fig. 5B) and at higher levels than other GFP$^+$ populations (fig. S7C), consistent with their identity as Ly6C^{hi} monocytes (*38*, *39*, *42*). These results suggested that key CCR2$^+$ cells could be myeloid cells.

Ly6C^{hi} monocyte accumulation paralleled the two waves of FRC CCL2 up-regulation seen after immunization. Monocyte numbers first increased at day 2 when CCL21$^-$ FRCs up-regulated CCL2 and further increased at day 9 when CCL21$^+$ FRCs up-regulated CCL2 (Fig. 2B and fig. S7D). GFP$^+$ cells in *Ccr2*-GFP mice were mainly in the T zone and medulla and colocalized with AFCs at all time points examined (fig. S7, E and F). The GFP$^+$ cells in these regions were composed of both round GFP^{hi} cells likely to be monocytes and elongated GFP^{med} cells presumed to be DCs (Fig. 5C). These results are consistent with a role for stromal CCL2 in positioning CCR2$^+$ myeloid cells to promote interactions with AFCs.

We asked the extent to which stromal CCL2 promoted lymph node accumulation of monocytes and other CCR2$^+$ cells. At day 15 after immunization, *Ccl2*$^{-/-}$ mice had reduced lymph node Ly6C^{hi} and Ly6C^{med} monocytes without an effect in other myeloid populations (Fig. 5D). Homeostatic popliteal and brachial *Ccl2*$^{-/-}$ lymph nodes showed fewer Ly6C^{hi} monocytes (fig. S8A). Although these results could reflect the critical role of bone marrow stromal CCL2 in mobilizing monocytes from bone marrow into circulation (*20*, *42*, *43*), transplanted *Ccl2*$^{-/-}$ lymph nodes also showed a specific reduction in Ly6C^{hi} and Ly6C^{med} monocytes (Fig. 5E). These results suggested a distinct role for lymph node stromal CCL2 in mediating lymph node monocyte accumulation, by either entry or retention, and supported the possibility that CCR2$^+$ monocytes limit AFC survival.

We confirmed that CCR2$^+$ cells regulated AFCs during days 12 to 15 by treating *Ccr2*-DTR mice (*44*) with diphtheria toxin (DT) during this window (fig. S8B). DT depleted 90% of CCR2$^+$ cells (Fig. 5F) and, consistent with the work of others (*16*) (*17*), led to increased AFC numbers (Fig. 5G). Total B and germinal center B cell numbers were not affected (Fig. 5G), and the AFC increase was associated with decreased apoptosis and unchanged proliferation (Fig. 5, G and H). Our results together suggested that stromal CCL2 limits AFC survival late during immune responses, at least in part, by mediating lymph node accumulation of CCR2$^+$ cells.

To better understand the importance of monocytes as key CCR2$^+$ cells, we depleted monocytes with anti-Gr1, which recognizes Ly6C and Ly6G (*45*, *46*), between days 12 and 15 (fig. S8C). Ly6C^{hi} monocytes and Ly6C^{med}Ly6G$^+$ neutrophils were well depleted, whereas Ly6C^{med} Ly6G$^-$ monocytes were partially depleted (Fig. 5, I and J). This led to increased AFC numbers and decreased AFC apoptosis without affecting the numbers of B and germinal center B cells (Fig. 5, K and L). These results were not attributable to neutrophil depletion, as their depletion with anti-Ly6G had no effect on AFCs (fig. S8, D to G). These results point to monocytes as key CCR2$^+$ cells that limit lymph node AFC survival during the later stages of antibody responses.

We asked whether monocytes are sufficient to limit AFC numbers in our model. *Ccr2*$^{-/-}$ mice showed greatly reduced lymph node monocyte numbers (Fig. 6A), increased B cell, germinal center B cell, and AFC numbers, and increased AFC survival (Fig. 6, B and C), which further supported a role for monocytes in regulating AFCs. The effects on B cell responses were greater than in *Ccl2*$^{-/-}$ mice, potentially reflecting additive roles of CCL2 with other CCR2 ligands such as CCL7 (*43*, *47*). We transferred CD45.1 Ly6C^{hi} monocytes

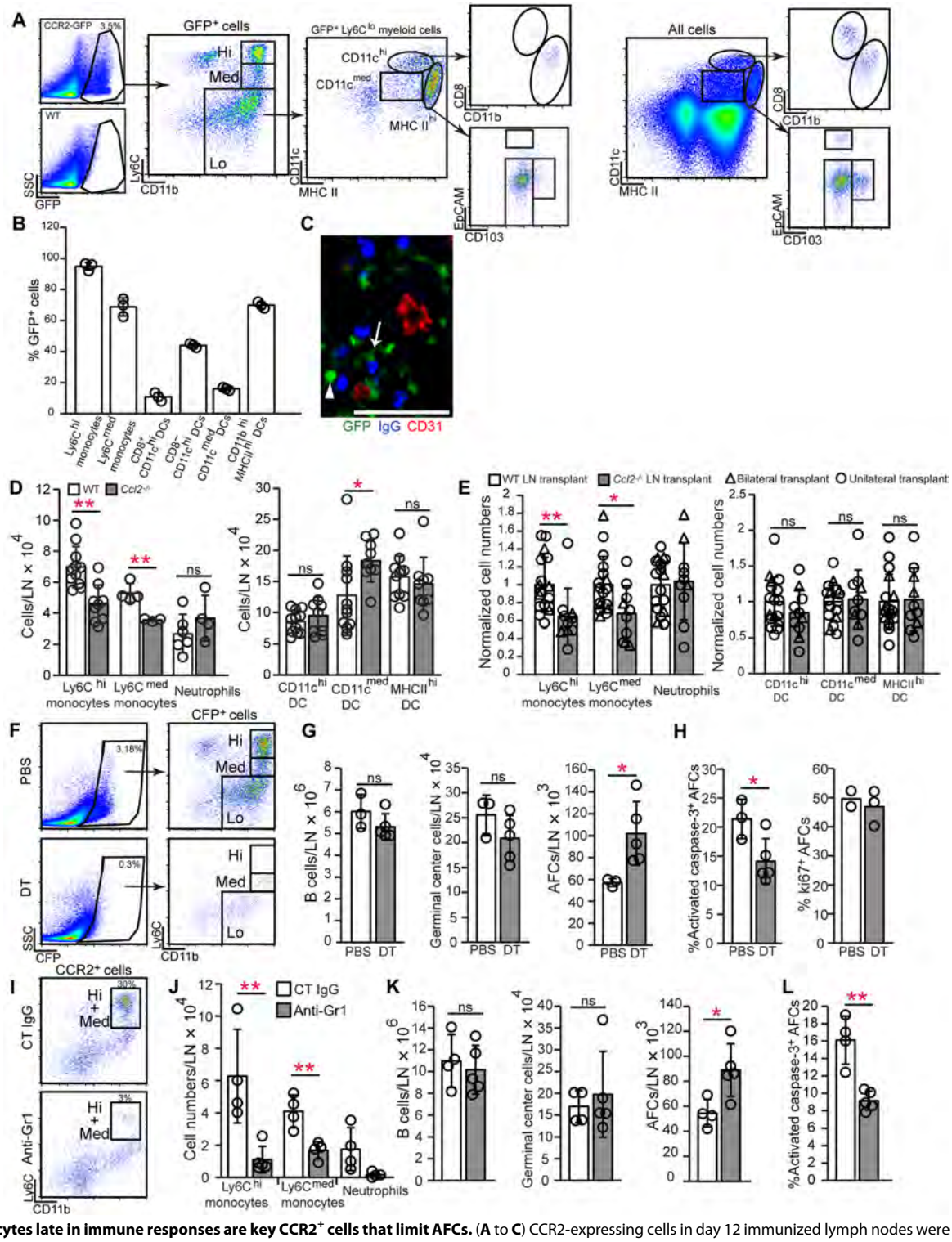

Fig. 5. Monocytes late in immune responses are key CCR2$^+$ cells that limit AFCs. (**A** to **C**) CCR2-expressing cells in day 12 immunized lymph nodes were characterized using *Ccr2*-GFP reporter mice. (A) Representative flow cytometry plots show GFP$^+$ subsets. (B) Percentage of CCR2$^+$ cells in indicated myeloid populations. (C) Frozen section stained for indicated markers. Arrowhead points to round CCR2^{hi} cell; arrow points to DC-shaped CCR2^{med} cell. Scale bar, 100 μm. (**D** and **E**) Numbers of indicated myeloid populations at day 15 after immunization in (D) WT and *Ccl2*$^{-/-}$ popliteal nodes and (E) WT and *Ccl2*$^{-/-}$ popliteal nodes transplanted into WT recipients. (**F** to **H**) CCR2-DTR-CFP mice were immunized with OVA-Alum on day 0, treated with DT on days 12 and 14, and examined on day 15. (F) Flow cytometry plots showing CCR2$^+$ cell depletion. (G) Numbers of indicated cells. (H) Percentages of AFCs that are activated caspase-3$^+$ and ki67$^+$. (**I** to **L**) WT mice were injected with anti-Gr1 or control IgG on days 12 to 14 after OVA-Alum and examined on day 15. (I) Flow cytometry plots showing CCR2$^+$ cell depletion. (J) Numbers of indicated myeloid populations. (K) Numbers of indicated cells. (L) Percentage of AFCs that are activated caspase-3$^+$. (A, F, and I) Fluorescence scale is $\log_{10}$. (B, D, E, G, H, and J to L) Each symbol represents one mouse; $n = 3$ to 17 per condition; data are from 6 to 11 (D and E) and 2 (B, G, H, and J to L) experiments. *$P < 0.05$, **$P < 0.01$ by two-tailed unpaired Student's t test. Error bars represent SD.

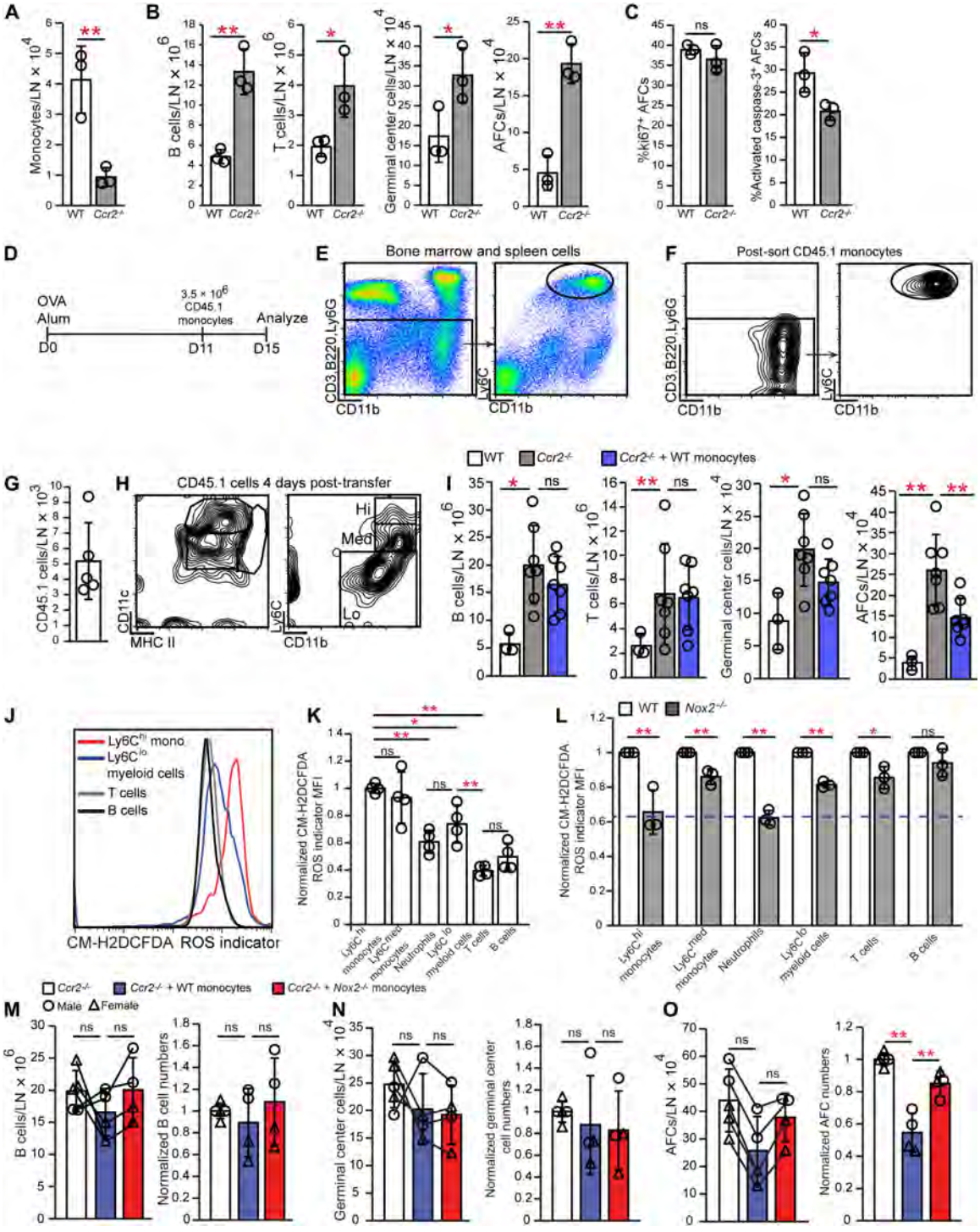

Fig. 6. Monocytes limit AFCs in a NOX2-dependent manner. (**A** to **C**) WT and *Ccr2*$^{-/-}$ mice were immunized on day 0, and draining popliteal nodes were examined on day 15. Numbers of (A) Ly6C^{hi} monocytes and (B) indicated cells. (C) Percentage of AFCs that are ki67^{+} and activated caspase-3^{+}. (**D** to **I**) CD45.1^{+} Ly6C^{hi} monocytes were transferred into *Ccr2*$^{-/-}$ recipients at day 11 after OVA-Alum, as in (D). (E) Gating strategy for monocyte sorting. (F) Sorted monocyte characterization. (G and H) Recovered donor cell numbers (G) and characterization (H). (I) Numbers of indicated cells. (**J** to **L**) Cells from day 15 nodes were loaded with the fluorescent ROS indicator CM-H2DCFDA. (J) Fluorescence in indicated cells. (K to L) Relative ROS expression. Mean fluorescence intensity (MFI) in each population was normalized to the MFI of (K) Ly6C^{hi} monocytes or (L) each WT population. Dashed line represents the fluorescence of WT B cells relative to that of WT Ly6C^{hi} monocytes. (**M** to **O**) WT or NOX2-deficient monocytes were transferred into *Ccr2*$^{-/-}$ recipients on day 11 after immunization and analyzed on day 15. Absolute numbers and numbers normalized to those of *Ccr2*$^{-/-}$ mice that received no cells are both shown. Lines connecting the symbols denote the matched mice from a given experiment. (M) B cells, (N) germinal center B cells, and (O) AFCs. (A to C, G, I, and K to O) Each symbol represents one mouse; $n = 3$ to 7 per condition. Data are from one (A to C) experiment, representative of four similar experiments [see (I)]. Data are from two (K), three (L), four (M to O), five (G), and seven (I) experiments. *$P < 0.05$, **$P < 0.01$ by two-tailed unpaired Student's t test. Error bars represent SD.

on day 11 after OVA-Alum and examined the *Ccr2*$^{-/-}$ recipients at day 15 (Fig. 6, D to F). Transferred cells that were recovered from the immunized lymph nodes (Fig. 6G) expressed medium to low levels of Ly6C and were CD11c$^{med\text{-}hi}$ and MHCII^{med} (Fig. 6H), suggesting some degree of differentiation. Monocyte transfer reduced AFCs without affecting germinal center B or T cell numbers (Fig. 6I). These results complement previous findings showing that monocyte transfer at the time of viral infection could reduce AFC responses (*19*). Together, our results suggested that CCR2^{+} monocytes limit AFC accumulation in the later stages of antibody responses and are key mediators of the stromal CCL2 effect on AFCs.

Monocyte NOX2 contributes to ROS production and AFC regulation

Myeloid cells can limit T cell responses via ROS (*48*), and monocytes showed high levels of ROS when compared with lymphocytes (Fig. 6, J and K). NADPH oxidase is a major contributor to the generation of myeloid cell ROS that is released extracellularly (*49*) and, interestingly, global deficiency of the *Nox2* gene that encodes the NOX2/gp91^{phox} subunit of NADPH oxidase in a lupus model increased plasmablast numbers (*50*). Given that monocytes from *Nox2*$^{-/-}$ mice (*51*) showed reduced ROS levels at day 15 after immunization (Fig. 6L), we examined their ability to limit AFC responses. *Nox2*$^{-/-}$ monocytes were less able than WT monocytes to limit AFCs when transferred into *Ccr2*$^{-/-}$ mice at day 11 (Fig. 6, M to O). Our results suggested that monocytes limit AFC accumulation via NOX2-dependent ROS.

Stromal CCL2 modulates monocyte ROS production

In addition to regulating monocyte accumulation and positioning in lymph nodes, CCL2 could potentially modulate monocyte ROS expression. Monocytes and potential monocyte-derived cells that can express CCR2 such as (CD11b^{+}) Ly6C^{med} or Ly6C^{lo} cells showed decreased ROS levels in *Ccl2*$^{-/-}$ mice (Fig. 7, A and B), leading us to ask whether lymph node stromal CCL2 can directly regulate monocyte ROS production. Cultured FRCs expressed CCL2 (Fig. 7C), and we added supernatant from WT or *Ccl2*$^{-/-}$ FRC cultures to sorted monocytes and observed that monocytes had lower intracellular ROS when exposed to *Ccl2*$^{-/-}$ FRC supernatant (Fig. 7D). In addition, WT FRC supernatant increased extracellular ROS levels when added to monocytes (Fig. 7E), whereas *Ccl2*$^{-/-}$ FRC supernatant was less able to do so (Fig. 7E), consistent with the idea that FRC-derived CCL2 can modulate monocyte ROS generation. These in vitro results suggested that, in addition to monocyte accumulation and positioning, stromal CCL2 can directly modulate monocyte function, inducing ROS generation and release that can limit AFC survival.

We next tried to understand how CCL2 modulated monocyte ROS levels and how ROS might regulate AFCs. *Ccl2*$^{-/-}$ FRC supernatant induced a slight reduction in monocyte NOX2 levels (Fig. 7F), suggesting that CCL2 may potentially regulate ROS monocyte production, at least in part, by modulating NOX2 expression. We also found that FRCs sorted from immunized WT and *Ccl2*$^{-/-}$ lymph nodes expressed BAFF at similar levels (fig. S8H), suggesting that the larger B cell response with CCL2 deficiency is not due to FRC BAFF overexpression.

Stromal CCL2 expression is regulated by altering vascular permeability

We examined for factors that up-regulated stromal CCL2 in stimulated lymph nodes. Type I interferon limits B cell responses early during viral infections (*19*, *52*), but interferon-α receptor antibody blockade between days 5 and 9 or days 11 and 15 after immunization did not alter FRC CCL2 expression (fig. S9, A to D).

Because stromal CCL2 was high in vascular-rich areas, we asked whether inflammation-associated vascular permeability increases that occur in lymph nodes (*53*) can modulate stromal CCL2, potentially by increasing exposure to intravascular contents. VE-cadherin mediates endothelial barrier integrity, and anti–VE-cadherin (*54*) injected into hind footpads could induce local permeability changes, increasing interstitial accumulation of systemically injected Evans blue dye in popliteal but not brachial nodes (Fig. 8A). Anti–VE-cadherin increased CCL2 expression in FRCs and LECs but not in monocytes or CD11b^{+}Ly6C^{lo} cells (Fig. 8, B and C), and this was associated with increased monocytes, without affecting the numbers of total lymph node cells, other myeloid cells, or lymphocytes (Fig. 8D and fig. S9, E and F). FRCs had an altered phenotype upon anti–VE-cadherin treatment, with modestly increased PDPN and a larger increase in Sca1 expression (fig. S9, G and H). FRC numbers were unchanged (fig. S9I). The Sca1 up-regulation was mainly in the BP3^{+} population (fig. S9J), and other markers such as CD34, SMA, and CCL21 did not change (fig. S9, K and L). These results suggested that increasing vascular permeability up-regulated stromal CCL2, which increased monocyte accumulation.

Angiopoietin1 (Ang1) reduces vascular permeability by acting on endothelial cell junctions (*55*, *56*), and Ang1 in immunized mice reduced CCL2 expression by FRCs but not by LECs, monocytes, or CD11b^{+}Ly6C^{lo} cells (Fig. 8, E and F). Ang1 also increased B cell and AFC numbers and AFC survival (Fig. 8, G to I). These results are consistent with the idea that reducing vascular permeability reduced stromal CCL2 expression and consequently increased AFC survival.

Although anti–VE-cadherin and Ang1 can modulate the permeability of both blood and lymphatic vessels, blood serum caused up-regulation of both FRC PDPN and CCL2 (fig. S9M), similar to the effects of anti–VE-cadherin in vivo (Fig. 8, B and C). These results are consistent with the idea that increased blood vessel permeability and consequent exposure to serum may contribute to up-regulating FRC CCL2 in the vascular-rich areas of lymph nodes.

DISCUSSION

Here, we showed that the lymph node stromal compartment can function to limit AFC survival. High stromal CCL2 expression colocalized with AFCs and CCR2^{+} cells in the T zone and medulla, and lymph node transplantation experiments indicated the importance of stromal CCL2. FRCs express higher levels of CCL2 than LECs and up-regulated CCL2 during the later stages of the antibody response. Together with previous findings that FRCs have AFC-supportive functions (*13*–*15*), our current results suggest that the stromal compartment plays dual roles in AFC regulation.

Our finding that FRCs express high levels of CCL2 is in agreement with recent analyses of FRC gene expression patterns (Immgen.org) (*5*, *57*). Furthermore, Cyster and colleagues' recent single-cell RNA sequencing analysis of lymph node stromal cells at days 0 and 15 after lymphocytic choriomeningitis virus (LCMV)–Armstrong infection (*26*) showed that CCL2 is one of the differentially expressed genes that mark the CXCL9^{+} subset. CXCL9-expressing FRCs were suggested to represent an activated FRC population, and CXCL9 is found in the interfollicular regions, the T zone, and the medulla (*26*, *58*). That CCL2 is up-regulated upon lymph node activation and high

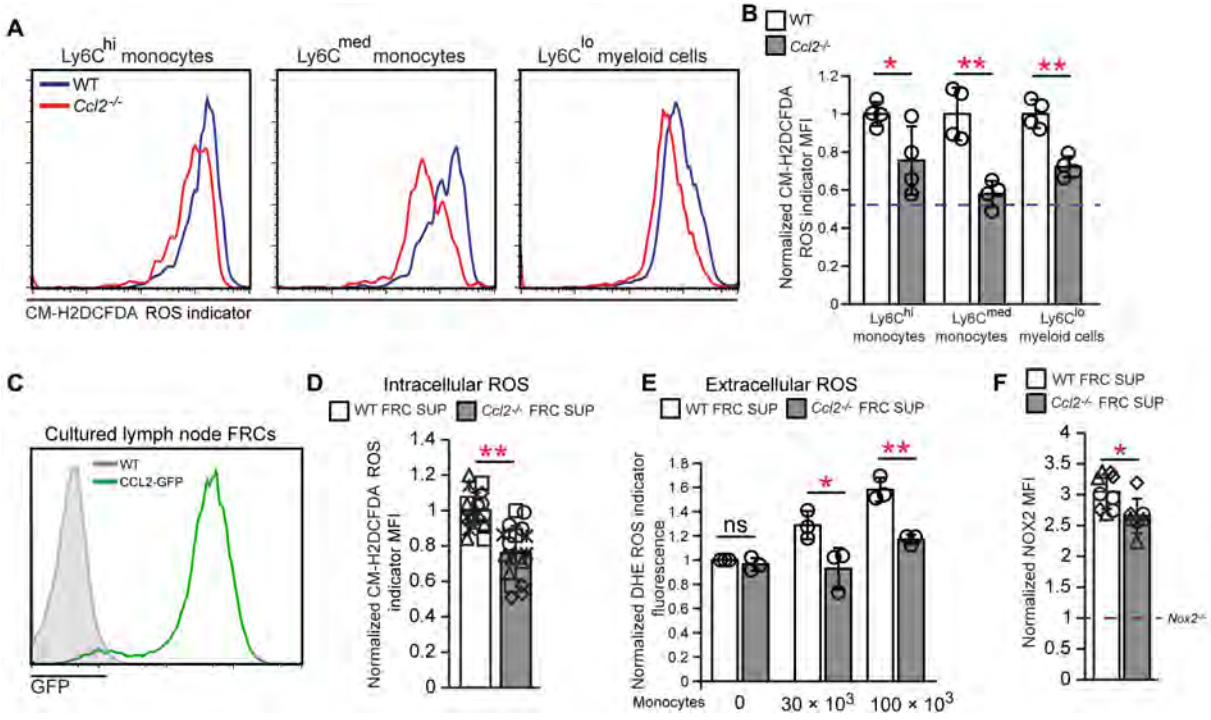

Fig. 7. FRC CCL2 regulates monocyte ROS production. (**A** and **B**) Day 15 OVA-Alum immunized WT or *Ccl2*$^{-/-}$ lymph node cells were loaded with CM-H2DCFDA. (A) Fluorescence in indicated cells. (B) Relative ROS levels as indicated by MFI of each *Ccl2*$^{-/-}$ population normalized to MFI in WT cells. Data are from two experiments. Dashed line represents fluorescence of WT B cells relative to that of WT Ly6C^{hi} monocytes. (**C**) GFP expression by FRCs cultured from WT and CCL2-GFP mice. (**D** to **F**) Monocytes were incubated with WT or *Ccl2*$^{-/-}$ FRC supernatants, and then cells and supernatants were assayed as indicated. (D) Relative intracellular ROS in monocytes, as indicated by MFI after CM-H2DCFDA loading. (E) Extracellular ROS in supernatants, as indicated by fluorescence of the superoxide indicator DHE in each supernatant normalized to the value of the WT supernatant without monocytes. (F) Normalized MFI of anti-NOX2 staining in monocytes. Dashed line represents the level of NOX2 antibody staining in *Nox2*$^{-/-}$ sorted monocytes that was used as a negative control and to which the other MFIs were normalized to. (A and C) Fluorescence scale is $\log_{10}$. (D to F) Data are from five (D) and three (E and F) independent experiments. (D and F) Each symbol is an individual well, with different symbols denoting independent experiments. (E) Each symbol represents the average of two to three wells from an experiment. *$P < 0.05$, **$P < 0.01$ by two-tailed unpaired Student's *t* test. Error bars represent SD.

expression is localized to some of the same areas as CXCL9 suggests that at least some CCL2-expressing FRCs are in the CXCL9-expressing population (*26*). We speculate that differential cytokine expression by different FRC subsets likely contributes to the dual nature of FRCs in both supporting and limiting AFCs.

In addition to a role in modulating AFC survival, there are likely other roles for stromal CCL2 in lymph nodes. For example, CCL2 expressed at lower levels by FRCs at homeostasis may contribute to the CCR2-dependent accumulation of monocyte-derived macrophages in the T zone (*59*). These macrophages expanded by proliferation rather than recruitment during immune responses, further supporting the idea that the up-regulated FRC CCL2 during immune responses has a distinct function, in part, by recruiting blood-borne Ly6C^{hi} monocytes to limit AFC accumulation. We also observed that CCL2 is rapidly up-regulated at day 2 in CCL21^{-} FRCs presumed to be part of interfollicular or medullary compartments. This early stromal CCL2 up-regulation coincides with an early wave of Ly6C^{+} monocyte infiltration, which is involved in stimulating the initial lymph node stromal proliferation (*41*), whereas the delayed CCL2 up-regulation in CCL21^{+} FRCs is temporally associated with the AFC response. This suggests that there may be distinct roles for CCL2 expressed by different subsets of FRCs over the course of immune responses.

Our work also complements and extends recent data showing roles for myeloid cells in regulating AFC responses. Giordano *et al.* (*17*) and Sammicheli *et al.* (*19*) showed that monocyte manipulation at the initiation of immune responses increased antibody responses, suggesting that monocytes could act on the nascent B cell response and/or subsequent AFCs. Our experiments showed that CCR2^{+} cell depletion, anti-Gr1 treatment, and monocyte transfer at day 11 or 12 after OVA-Alum immunization affected AFC but not total B cell and germinal center cell numbers, suggesting that monocytes may regulate AFCs specifically at this later stage. These recent studies also implicated monocyte-derived iNOS in regulating AFCs, and our finding that monocyte NOX2 is important may reflect the multiple mechanisms by which monocytes can regulate AFC responses. Fooksman *et al.* (*16*) also observed that CCR2^{+} cell depletion at 4 days into a secondary response led to greater AFC numbers by day 7, the time of peak AFC accumulation in their system, although they did not detect a role for apoptosis (by annexin V staining) or monocytes (by anti-Gr1 treatment). We speculate that our results differ because of differences in the time window being examined. Collectively, our study, in conjunction with these previous studies, suggests that different CCR2^{+} cells may play distinct roles in modulating AFCs at different time points in antibody responses.

Our results suggest that vessel-rich areas of lymph nodes such as the cortical ridge, the T zone vascular cords, and the medulla can be specialized microenvironments, in part, due to the dynamic activity of the vasculature. The lymph node vasculature can regulate

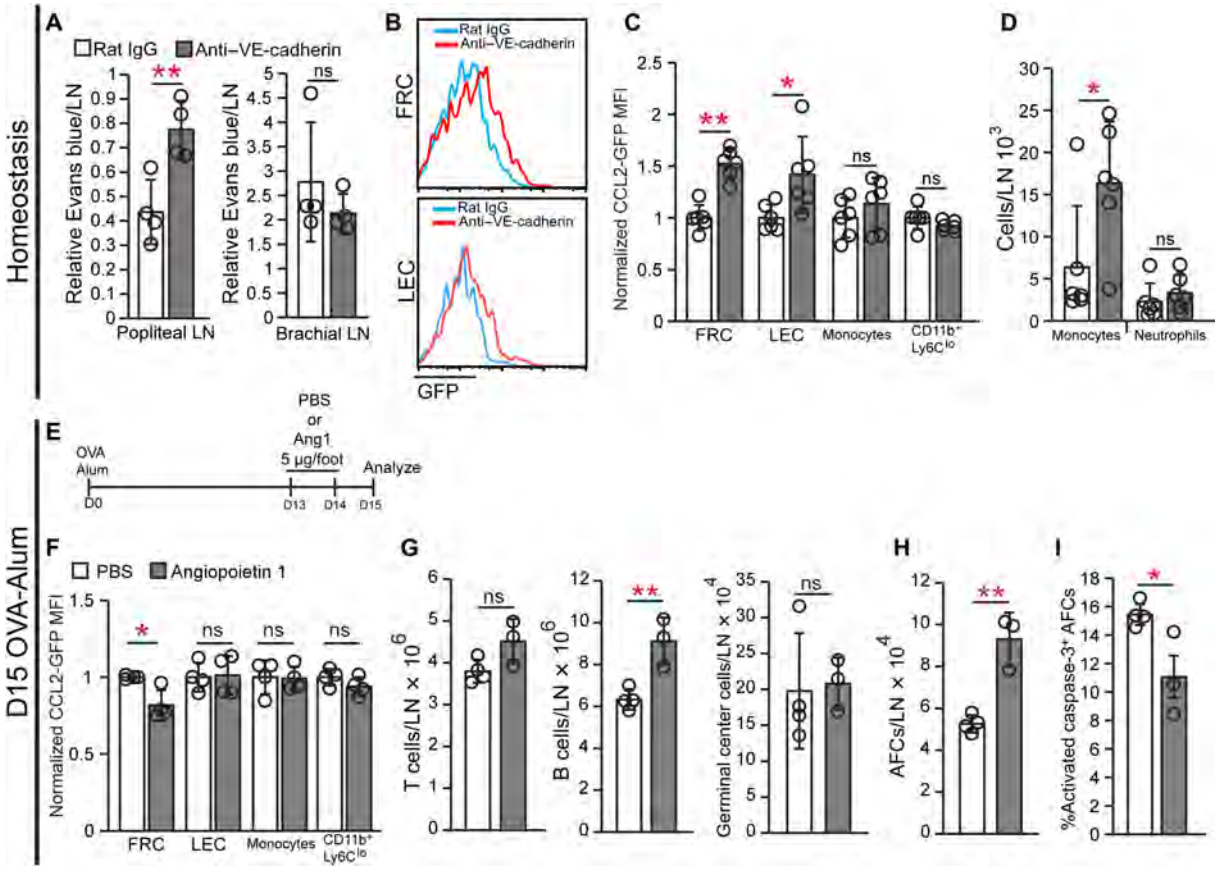

Fig. 8. Vascular permeability regulates stromal CCL2 expression. (**A** to **D**) Homeostatic WT (A) or CCL2-GFP (B to D) mice were injected with anti–VE-cadherin or control IgG in footpads, and draining popliteal (A to D) and nondraining brachial (A) lymph nodes were analyzed 24 hours later. (A) Vascular permeability measurement. (B) GFP in FRCs and LECs of CCL2-GFP mice. (C) Normalized GFP MFI in indicated populations. (D) Numbers of indicated cells. (**E** to **I**) CCL2-GFP (F) or WT (G to I) mice received Ang1 in footpads at days 13 and 14 after OVA-Alum, and popliteal nodes were harvested on day 15, as in (E). (F) Normalized GFP MFI in indicated populations. (G and H) Numbers of indicated cells. (I) Percentage of AFCs that are activated caspase-3$^+$. (A, C, D, and F to I) Each symbol represents one mouse; $n = 3$ to 6 per condition. Data are from two (A, C, D, and F) and three (G to I) independent experiments. $^*P < 0.05$, $^{**}P < 0.01$ by two-tailed unpaired Student's t test. Error bars represent SD.

immunity by controlling cellular trafficking (*60*) and by direct effects on lymphocytes (*61*). Our results suggest that vascular functions such as altered permeability also offer opportunities to affect immune responses, in part, by modulating stromal function.

Our results have implications for better treating autoimmune and inflammatory diseases. Although CCL2- and CCR2-expressing cells have been implicated in tissue damage in conditions such as lupus and inflammatory arthritis (*62*–*67*), targeting a CCL2-CCR2 axis globally has not been a successful strategy (*68*). Disrupting the regulatory role of lymph node stromal CCL2 could have been a contributing factor, and bone marrow mesenchymal stromal cell CCL2 can limit bone marrow plasma cell antibody production in a direct manner (*69*, *70*). In addition, swift production of CCL2 by FRCs in omental fat–associated lymphoid clusters is crucial for the induction of peritoneal immunity (*71*) and very early CCL2 relayed from inflamed tissues to the draining nodes (*72*) can signal the onset of immune responses; thus, disrupting CCL2 globally may be detrimental to protective immunity. Bone marrow mesenchymal stromal cells from patients with lupus expressed lower levels of CCL2 (*70*), suggesting the possibility that lymph node FRC CCL2 expression may also be reduced, contributing to autoimmunity. Better understanding how the source and context of CCL2 production determines its function and how factors such as vascular permeability shape the stromal microenvironment will better inform potential targeting of CCL2 and other CCR2 ligands in disease. Consistent with this idea, our results point to a need to consider potential dual roles of stromal elements when considering how to design stromal-targeting strategies.

MATERIALS AND METHODS

Study design

The purpose of this study was to understand expression, function, and regulation of lymph node stromal CCL2. The subjects were laboratory mice. We used immunofluorescence microscopy to visualize cell localization and flow cytometry to quantify cell numbers. For in vivo experiments, sample size of $n = 3$ to 17 animals per condition evaluated in 1 to 11 independent experiments was found to be optimal for statistical analysis. For in vitro experiments, sample size of $n = 2$ to 3 wells per condition per experiment in three to five independent experiments was used.

Mice

Mice between 6 and 12 weeks were used unless otherwise specified. We used C57Bl/6, CCL2$^{-/-}$ (*73*), and Nox2$^{-/-}$ (*51*) mice from The

Jackson Laboratory (Bar Harbor, ME) and CD45.1$^+$ (B6.SJL-*Ptprc*^{a}*Pepc*^{b}/BoyCrl) mice from Charles River (Wilmington, MA) or our own breeding colony. CCL2-GFP (*20*) and CCR2-DTR (*44*) mice were bred at our facility. *Ccl19*-Cre mice (*30*) were crossed at our facility with ROSA26-YFP$^{f/STOP/f}$ mice (The Jackson Laboratory) (*74*). All animal procedures were performed in accordance with the regulations of the Institutional Animal Care and Use Committee at Weill Cornell Medicine (New York, NY).

Mouse immunization and treatments

Mice were immunized in the hind footpads with 30 μg of OVA adsorbed to 30 μl of Alum. DT (Enzo Life Sciences, Farmingdale, NY; 250 ng of DT per dose) was injected intraperitoneally. Anti-Gr1 (RB6-8C5), anti-Ly6G (1A8), and isotype controls (LTF-2, 2A3) (all BioXCell, West Lebanon, NH; 250 μg per dose) were injected intraperitoneally. Anti–VE-cadherin (BV13) or rat IgG (both Thermo Fisher Scientific, Waltham, MA; 25 μg) and Ang1 (PeproTech, Rocky Hill, NJ; 5 μg) were injected in footpad.

Lymph node transplantation

For lymph node transplantations (*31*), donor popliteal nodes were harvested after euthanasia, before transplantation. Recipient mice were anesthetized and injected with 1% Evans blue in dorsal footpads to localize popliteal lymph nodes, which were removed through incisions in the popliteal fossa and with minimal disruption to the surrounding fat pad and blood vessels. Donor lymph nodes were placed into the fossa, and skin was closed using 3-0 nonabsorbable sutures.

Vascular permeability assay

Mice were injected retroorbitally with 2% Evans blue, euthanized after 90 min, and perfused with 30 ml of phosphate-buffered saline (PBS) before lymph node harvest. Evans blue was extracted in 200 μl of formamide at 60°C overnight and quantified by spectrophotometry (680-nm fluorescence emission intensity, 620-nm excitation) with titration curve.

Flow cytometry staining and quantification

Lymph nodes were harvested, minced, and digested with type II collagenase (Worthington, Lakewood, NJ) as described (*75*). The following antibodies were used: anti-CD45, CD31 (both BD Biosciences, San Jose, CA), PDPN, BP3, Sca1, CD11b, CD11c, I-Ab, Ly6C, Ly6G, CD3, B220 (all BioLegend, San Diego, CA), CD34, GFP (both Thermo Fisher Scientific), CCL21, CCL2, CCR2, activated caspase-3 (all R&D Systems, Minneapolis, MN), and rabbit and goat IgG (Jackson Immunoresearch, West Grove, PA). Peanut agglutinin (PNA) was from Vector Laboratories, Burlingame, CA. BD Cytofix/Cytoperm kit was used for intracellular staining. The Foxp3 buffer set (Thermo Fisher Scientific) was used for ki67 staining after AFC staining.

Cells per lymph node were calculated by multiplying the percentage of total gated population to lymph node cell count. For normalized experiments where there was more than one control sample, the control values were averaged and the individual control and experimental samples were normalized to this average value.

ROS assay

Intracellular and extracellular ROS were measured using CM-H2DCFDA and dihydroethidium (DHE), respectively (both Thermo Fisher Scientific), according to the manufacturer's specifications.

Tissue section staining and microscopy

CCL2-GFP tissues were fixed in 4% paraformaldehyde (1 hour on ice), cryoprotected in 30% sucrose, and frozen in optimal cutting temperature (OCT) embedding medium (Tissue-Tek, Torrance, CA). Other tissues were fresh-frozen in OCT. Antibodies are as used for fluorescence-activated cell sorting (FACS) except anti-CXCL13 (R&D Systems), ERTR7 (Santa Cruz Biotechnology, Santa Cruz, CA), GFP-Alexa488 and fluorescein isothiocyanate (FITC)–Alexa488 (both Thermo Fisher Scientific), and goat-Alexa488, rat-rhodamine, Armenian hamster-AMCA (aminomethylcoumarin), rabbit-rhodamine, mouse IgG-biotin, and streptavidin-rhodamine/AMCA (all Jackson Immunoresearch).

ELISpot assay

ELISpot (enzyme-linked immunospot assay) detection of anti-OVA–secreting cells was performed as described (*13*). Wells were coated with 0.1% OVA (Sigma-Aldrich, St. Louis, MO), cells were incubated at 37°C for 4 hours, and secreted anti-OVA was detected using anti-mouse IgG-biotin (Jackson Immunoresearch), streptavidin-alkaline phosphatase (Jackson Immunoresearch), and 5-bromo-4chloro-3-indolyl-phosphate (Sigma-Aldrich).

Cell sorting

For monocyte isolation, cells from long bones and spleen were pooled and depleted with anti-CD3/B220/Ly6G via magnetic selection (Miltenyi Biotec, Bergisch Gladbach, Germany), and Ly6C^{hi} CD11b ^{hi} cells were sorted using a BD Influx (BD Biosciences). For FRC sorting, cells from draining lymph nodes 15 days after immunization were pooled and depleted with anti-CD45/CD31, and CD45$^-$ CD31$^-$ PDPN$^+$ cells were sorted into RLT buffer (Qiagen, Venlo, The Netherlands) for RNA extraction.

Real-time PCR

RNA was extracted (RNeasy Mini Kit, Qiagen), complementary DNA (cDNA) was synthesized (iScript kit, Bio-Rad, Hercules, CA), and real-time polymerase chain reaction (PCR) (iQ SYBR Green Supermix kit, Bio-Rad) was performed using primers for BAFF and GAPDH (glyceraldehyde-3-phosphate dehydrogenase) [as in (*13*)].

In vitro experiments

Peripheral lymph node FRCs from homeostatic mice were cultured as described (*13*). Collagenase-digested lymph node cells were plated in RPMI/10% fetal calf serum, washed of nonadherent cells at day 5, harvested at day 7, and depleted with anti-CD45/CD31, resulting in FRC purity over 97%. FRCs were cultured in 96-well plates at 7500 cells per well per 100 μl. Supernatants were collected at 2 days and stored at −20°C until use. For experiments, supernatant was added to monocytes for 24 hours before harvest.

Statistics

Statistical significance was determined using two-tailed unpaired Student's *t* test; $P < 0.05$ was considered significant. Error bars represent SD.

SUPPLEMENTARY MATERIALS

immunology.sciencemag.org/cgi/content/full/5/45/eaaw0693/DC1

Fig. S1. Characterization of BP3$^+$ and BP3$^{lo\text{-}neg}$ FRCs.

Fig. S2. Characterization of lymph node AFC responses and localization after OVA-Alum.

Fig. S3. Characterization of immune cell populations in homeostatic and immunized *Ccl2*$^{-/-}$ lymph nodes and spleens.
Fig. S4. YFP expression in *Ccl19*-Cre;YFP$^{f/STOP/f}$ FRCs at day 15 after OVA-Alum.
Fig. S5. Transplanted lymph nodes show normal organization.
Fig. S6. Analysis of optimal transplants and immune responses.
Fig. S7. Further characterization of CCR2 expression and CCR2^{+} cell identity, numbers, and localization after immunization.
Fig. S8. Monocyte numbers are lower in homeostatic *Ccl2*$^{-/-}$ lymph nodes, and neutrophils do not play a role in limiting antibody responses.
Fig. S9. Effects of interferon receptor blockade on stromal CCL2, anti–VE-cadherin on cell populations and FRC phenotype, and serum on FRC CCL2.
Data file S1.

View/request a protocol for this paper from *Bio-protocol*.

REFERENCES AND NOTES

1. J. E. Chang, S. J. Turley, Stromal infrastructure of the lymph node and coordination of immunity. *Trends Immunol.* **36**, 30–39 (2015).
2. Y. O. Alexandre, S. N. Mueller, Stromal cell networks coordinate immune response generation and maintenance. *Immunol. Rev.* **283**, 77–85 (2018).
3. A. L. Fletcher, S. E. Acton, K. Knoblich, Lymph node fibroblastic reticular cells in health and disease. *Nat. Rev. Immunol.* **15**, 350–361 (2015).
4. D. C. Dasoveanu, W. D. Shipman, J. J. Chia, S. Chyou, T. T. Lu, Regulation of lymph node vascular-stromal compartment by dendritic cells. *Trends Immunol.* 37, 764–777 (2016).
5. J. L. Gregory, A. Walter, Y. O. Alexandre, J. L. Hor, R. Liu, J. Z. Ma, S. Devi, N. Tokuda, Y. Owada, L. K. Mackay, G. K. Smyth, W. R. Heath, S. N. Mueller, Infection programs sustained lymphoid stromal cell responses and shapes lymph node remodeling upon secondary challenge. *Cell Rep.* **18**, 406–418 (2017).
6. B. F. Hoyer, K. Moser, A. E. Hauser, A. Peddinghaus, C. Voigt, D. Eilat, A. Radbruch, F. Hiepe, R. A. Manz, Short-lived plasmablasts and long-lived plasma cells contribute to chronic humoral autoimmunity in NZB/W mice. *J. Exp. Med.* **199**, 1577–1584 (2004).
7. J. William, C. Euler, S. Christensen, M. J. Shlomchik, Evolution of autoantibody responses via somatic hypermutation outside of germinal centers. *Science* **297**, 2066–2070 (2002).
8. S. Chyou, S. Tian, E. H. Ekland, T. T. Lu, Normalization of the lymph node T cell stromal microenvironment in lpr/lpr Mice is associated with SU5416-induced reduction in autoantibodies. *PLOS ONE* **7**, e32828 (2012).
9. S. L. Nutt, P. D. Hodgkin, D. M. Tarlinton, L. M. Corcoran, The generation of antibody-secreting plasma cells. *Nat. Rev. Immunol.* **15**, 160–171 (2015).
10. K. G. Smith, T. D. Hewitson, G. J. Nossal, D. M. Tarlinton, The phenotype and fate of the antibody-forming cells of the splenic foci. *Eur. J. Immunol.* **26**, 444–448 (1996).
11. D. R. Fooksman, T. A. Schwickert, G. D. Victora, M. L. Dustin, M. C. Nussenzweig, D. Skokos, Development and migration of plasma cells in the mouse lymph node. *Immunity* **33**, 118–127 (2010).
12. E. Mohr, K. Serre, R. A. Manz, A. F. Cunningham, M. Khan, D. L. Hardie, R. Bird, I. C. M. MacLennan, Dendritic cells and monocyte/macrophages that create the IL-6/APRIL-rich lymph node microenvironments where plasmablasts mature. *J. Immunol.* **182**, 2113–2123 (2009).
13. V. Kumar, D. C. Dasoveanu, S. Chyou, T. C. Tzeng, C. Rozo, Y. Liang, W. Stohl, Y. X. Fu, N. H. Ruddle, T. T. Lu, A dendritic-cell-stromal axis maintains immune responses in lymph nodes. *Immunity* **42**, 719–730 (2015).
14. Y. Zhang, L. Tech, L. A. George, A. Acs, R. E. Durrett, H. Hess, L. S. K. Walker, D. M. Tarlinton, A. L. Fletcher, A. E. Hauser, K. M. Toellner, Plasma cell output from germinal centers is regulated by signals from Tfh and stromal cells. *J. Exp. Med.* **215**, 1227–1243 (2018).
15. H.-Y. Huang, A. Rivas-Caicedo, F. Renevey, H. Cannelle, E. Peranzoni, L. Scarpellino, D. L. Hardie, A. Pommier, K. Schaeuble, S. Favre, T. K. Vogt, F. Arenzana-Seisdedos, P. Schneider, C. D. Buckley, E. Donnadieu, S. A. Luther, Identification of a new subset of lymph node stromal cells involved in regulating plasma cell homeostasis. *Proc. Natl. Acad. Sci. U.S.A.* **115**, E6826–E6835 (2018).
16. D. R. Fooksman, M. C. Nussenzweig, M. L. Dustin, Myeloid cells limit production of antibody-secreting cells after immunization in the lymph node. *J. Immunol.* **192**, 1004–1012 (2014).
17. D. Giordano, K. E. Draves, C. Li, T. M. Hohl, E. A. Clark, Nitric oxide regulates BAFF expression and T cell–independent antibody responses. *J. Immunol.* **193**, 1110–1120 (2014).
18. R. A. Sweet, K. M. Nickerson, J. L. Cullen, Y. Wang, M. J. Shlomchik, B cell–extrinsic *Myd88* and *Fcer1g* negatively regulate autoreactive and normal B cell immune responses. *J. Immunol.* **199**, 885–893 (2017).
19. S. Sammicheli, M. Kuka, P. Di Lucia, N. J. de Oya, M. De Giovanni, J. Fioravanti, C. Cristofani, C. G. Maganuco, B. Fallet, L. Ganzer, L. Sironi, M. Mainetti, R. Ostuni, K. Larimore, P. D. Greenberg, J. C. de la Torre, L. G. Guidotti, M. Iannacone, Inflammatory monocytes hinder antiviral B cell responses. *Sci. Immunol.* **1**, eaah6789 (2016).
20. C. Shi, T. Jia, S. Mendez-Ferrer, T. M. Hohl, N. V. Serbina, L. Lipuma, I. Leiner, M. O. Li, P. S. Frenette, E. G. Pamer, Bone marrow mesenchymal stem and progenitor cells induce monocyte emigration in response to circulating toll-like receptor ligands. *Immunity* **34**, 590–601 (2011).
21. T. Katakai, T. Hara, J. H. Lee, H. Gonda, M. Sugai, A. Shimizu, A novel reticular stromal structure in lymph node cortex: An immuno-platform for interactions among dendritic cells, T cells and B cells. *Int. Immunol.* **16**, 1133–1142 (2004).
22. U. H. von Andrian, T. R. Mempel, Homing and cellular traffic in lymph nodes. *Nat. Rev. Immunol.* **3**, 867–878 (2003).
23. M. D. Gunn, V. N. Ngo, K. M. Ansel, E. H. Ekland, J. G. Cyster, L. T. Williams, A B-cell-homing chemokine made in lymphoid follicles activates Burkitt's lymphoma receptor-1. *Nature* **391**, 799–803 (1998).
24. A. Link, T. K. Vogt, S. Favre, M. R. Britschgi, H. Acha-Orbea, B. Hinz, J. G. Cyster, S. A. Luther, Fibroblastic reticular cells in lymph nodes regulate the homeostasis of naive T cells. *Nat. Immunol.* **8**, 1255–1265 (2007).
25. K. M. Sitnik, K. Wendland, H. Weishaupt, H. Uronen-Hansson, A. J. White, G. Anderson, K. Kotarsky, W. W. Agace, Context-dependent development of lymphoid stroma from adult CD34^{+} adventitial progenitors. *Cell Rep.* **14**, 2375–2388 (2016).
26. L. B. Rodda, E. Lu, M. L. Bennett, C. L. Sokol, X. Wang, S. A. Luther, B. A. Barres, A. D. Luster, C. J. Ye, J. G. Cyster, Single-cell RNA sequencing of lymph node stromal cells reveals niche-associated heterogeneity. *Immunity* **48**, 1014–1028.e6 (2018).
27. A. Kallies, J. Hasbold, D. M. Tarlinton, W. Dietrich, L. M. Corcoran, P. D. Hodgkin, S. L. Nutt, Plasma cell ontogeny defined by quantitative changes in Blimp-1 expression. *J. Exp. Med.* **200**, 967–977 (2004).
28. K. Schumann, T. Lämmermann, M. Bruckner, D. F. Legler, J. Polleux, J. P. Spatz, G. Schuler, R. Förster, M. B. Lutz, L. Sorokin, M. Sixt, Immobilized chemokine fields and soluble chemokine gradients cooperatively shape migration patterns of dendritic cells. *Immunity* **32**, 703–713 (2010).
29. A. Braun, T. Worbs, G. L. Moschovakis, S. Halle, K. Hoffmann, J. Bölter, A. Münk, R. Förster, Afferent lymph-derived T cells and DCs use different chemokine receptor CCR7-dependent routes for entry into the lymph node and intranodal migration. *Nat. Immunol.* **12**, 879–887 (2011).
30. Q. Chai, L. onder, E. Scandella, C. Gil-Cruz, C. Perez-Shibayama, J. Cupovic, R. Danuser, T. Sparwasser, S. A. Luther, V. Thiel, T. Rülicke, J. V. Stein, T. Hehlgans, B. Ludewig, Maturation of lymph node fibroblastic reticular cells from myofibroblastic precursors is critical for antiviral immunity. *Immunity* **38**, 1013–1024 (2013).
31. J.-J. Huang, J. C. Gardenier, G. E. Hespe, G. D. García Nores, R. P. Kataru, C. L. Ly, I. Martínez-Corral, S. Ortega, B. J. Mehrara, Lymph node transplantation decreases swelling and restores immune responses in a transgenic model of lymphedema. *PLOS ONE* **11**, e0168259 (2016).
32. M. Ahrendt, S. I. Hammerschmidt, O. Pabst, R. Pabst, U. Bode, Stromal cells confer lymph node-specific properties by shaping a unique microenvironment influencing local immune responses. *J. Immunol.* **181**, 1898–1907 (2008).
33. R. E. Mebius, J. Brevé, G. Kraal, P. R. Streeter, Developmental regulation of vascular addressin expression: A possible role for site-associated environments. *Int. Immunol.* **5**, 443–449 (1993).
34. V. Angeli, F. Ginhoux, J. Llodrà, L. Quemeneur, P. S. Frenette, M. Skobe, R. Jessberger, M. Merad, G. J. Randolph, B cell-driven lymphangiogenesis in inflamed lymph nodes enhances dendritic cell mobilization. *Immunity* **24**, 203–215 (2006).
35. K. A. Soderberg, G. W. Payne, A. Sato, R. Medzhitov, S. S. Segal, A. Iwasaki, Innate control of adaptive immunity via remodeling of lymph node feed arteriole. *Proc. Natl. Acad. Sci. U.S.A.* **102**, 16315–16320 (2005).
36. I. F. Charo, S. J. Myers, A. Herman, C. Franci, A. J. Connolly, S. R. Coughlin, Molecular cloning and functional expression of two monocyte chemoattractant protein 1 receptors reveals alternative splicing of the carboxyl-terminal tails. *Proc. Natl. Acad. Sci. U.S.A.* **91**, 2752–2756 (1994).
37. N. V. Serbina, T. M. Hohl, M. Cherny, E. G. Pamer, Selective expansion of the monocytic lineage directed by bacterial infection. *J. Immunol.* **183**, 1900–1910 (2009).
38. F. Geissmann, S. Jung, D. R. Littman, Blood monocytes consist of two principal subsets with distinct migratory properties. *Immunity* **19**, 71–82 (2003).
39. S. Tamoutounour, M. Guilliams, F. Montanana Sanchis, H. Liu, D. Terhorst, C. Malosse, E. Pollet, L. Ardouin, H. Luche, C. Sanchez, M. Dalod, B. Malissen, S. Henri, Origins and functional specialization of macrophages and of conventional and monocyte-derived dendritic cells in mouse skin. *Immunity* **39**, 925–938 (2013).
40. M. Merad, P. Sathe, J. Helft, J. Miller, A. Mortha, The dendritic cell lineage: Ontogeny and function of dendritic cells and their subsets in the steady state and the inflamed setting. *Annu. Rev. Immunol.* **31**, 563–604 (2013).
41. F. Benahmed, S. Chyou, D. Dasoveanu, J. Chen, V. Kumar, Y. Iwakura, T. T. Lu, Multiple CD11c^{+} cells collaboratively express IL-1β to modulate stromal vascular endothelial growth factor and lymph node vascular-stromal growth. *J. Immunol.* **192**, 4153–4163 (2014).

42. N. V. Serbina, E. G. Pamer, Monocyte emigration from bone marrow during bacterial infection requires signals mediated by chemokine receptor CCR2. *Nat. Immunol.* **7**, 311–317 (2006).
43. C.-L. Tsou, W. Peters, Y. Si, S. Slaymaker, A. M. Aslanian, S. P. Weisberg, M. Mack, I. F. Charo, Critical roles for CCR2 and MCP-3 in monocyte mobilization from bone marrow and recruitment to inflammatory sites. *J. Clin. Invest.* **117**, 902–909 (2007).
44. T. M. Hohl, A. Rivera, L. Lipuma, A. Gallegos, C. Shi, M. Mack, E. G. Pamer, Inflammatory monocytes facilitate adaptive CD4 T cell responses during respiratory fungal infection. *Cell Host Microbe* **6**, 470–481 (2009).
45. T. J. Fleming, M. L. Fleming, T. R. Malek, Selective expression of Ly-6G on myeloid lineage cells in mouse bone marrow. RB6–8C5 mAb to granulocyte-differentiation antigen (Gr-1) detects members of the Ly-6 family. *J. Immunol.* **151**, 2399–2408 (1993).
46. I. R. Dunay, A. Fuchs, L. D. Sibley, Inflammatory monocytes but not neutrophils are necessary to control infection with *Toxoplasma gondii* in mice. *Infect. Immun.* **78**, 1564–1570 (2010).
47. T. Jia, N. V. Serbina, K. Brandl, M. X. Zhong, I. M. Leiner, I. F. Charo, E. G. Pamer, Additive roles for MCP-1 and MCP-3 in CCR2-mediated recruitment of inflammatory monocytes during *Listeria monocytogenes* infection. *J. Immunol.* **180**, 6846–6853 (2008).
48. S. Kusmartsev, Y. Nefedova, D. Yoder, D. I. Gabrilovich, Antigen-specific inhibition of $CD8^+$ T cell response by immature myeloid cells in cancer is mediated by reactive oxygen species. *J. Immunol.* **172**, 989–999 (2004).
49. K. Bedard, K.-H. Krause, The NOX family of ROS-generating NADPH oxidases: Physiology and pathophysiology. *Physiol. Rev.* **87**, 245–313 (2007).
50. A. M. Campbell, M. Kashgarian, M. J. Shlomchik, NADPH oxidase inhibits the pathogenesis of systemic lupus erythematosus. *Sci. Transl. Med.* **4**, 157ra141 (2012).
51. J. D. Pollock, D. A. Williams, M. A. C. Gifford, L. L. Li, X. du, J. Fisherman, S. H. Orkin, C. M. Doerschuk, M. C. Dinauer, Mouse model of X-linked chronic granulomatous disease, an inherited defect in phagocyte superoxide production. *Nat. Genet.* **9**, 202–209 (1995).
52. E. A. Moseman, T. Wu, J. C. de la Torre, P. L. Schwartzberg, D. B. McGavern, Type I interferon suppresses virus-specific B cell responses by modulating $CD8^+$ T cell differentiation. *Sci. Immunol.* **1**, eaah3565 (2016).
53. N. D. Anderson, A. O. Anderson, R. G. Wyllie, Microvascular changes in lymph nodes draining skin allografts. *Am. J. Pathol.* **81**, 131–160 (1975).
54. M. Corada, M. Mariotti, G. Thurston, K. Smith, R. Kunkel, M. Brockhaus, M. G. Lampugnani, I. Martin-Padura, A. Stoppacciaro, L. Ruco, D. M. McDonald, P. A. Ward, E. Dejana, Vascular endothelial-cadherin is an important determinant of microvascular integrity in vivo. *Proc. Natl. Acad. Sci. U.S.A.* **96**, 9815–9820 (1999).
55. G. Thurston, J. S. Rudge, E. Ioffe, H. Zhou, L. Ross, S. D. Croll, N. Glazer, J. Holash, D. M. McDonald, G. D. Yancopoulos, Angiopoietin-1 protects the adult vasculature against plasma leakage. *Nat. Med.* **6**, 460–463 (2000).
56. J. Gavard, V. Patel, J. S. Gutkind, Angiopoietin-1 prevents VEGF-induced endothelial permeability by sequestering Src through mDia. *Dev. Cell* **14**, 25–36 (2008).
57. D. Malhotra, A. L. Fletcher, J. Astarita, V. Lukacs-Kornek, P. Tayalia, S. F. Gonzalez, K. G. Elpek, S. K. Chang, K. Knoblich, M. E. Hemler, M. B. Brenner, M. C. Carroll, D. J. Mooney, S. J. Turley; Immunological Genome Project Consortium, Transcriptional profiling of stroma from inflamed and resting lymph nodes defines immunological hallmarks. *Nat. Immunol.* **13**, 499–510 (2012).
58. J. R. Groom, J. Richmond, T. T. Murooka, E. W. Sorensen, J. H. Sung, K. Bankert, U. H. von Andrian, J. J. Moon, T. R. Mempel, A. D. Luster, CXCR3 chemokine receptor-ligand interactions in the lymph node optimize CD4+ T helper 1 cell differentiation. *Immunity* **37**, 1091–1103 (2012).
59. M. Baratin, L. Simon, A. Jorquera, C. Ghigo, D. Dembele, J. Nowak, R. Gentek, S. Wienert, F. Klauschen, B. Malissen, M. Dalod, M. Bajénoff, T cell zone resident macrophages silently dispose of apoptotic cells in the lymph node. *Immunity* **47**, 349–362.e5 (2017).
60. J.-P. Girard, C. Moussion, R. Förster, HEVs, lymphatics and homeostatic immune cell trafficking in lymph nodes. *Nat. Rev. Immunol.* **12**, 762–773 (2012).
61. A. Mendoza, V. Fang, C. Chen, M. Serasinghe, A. Verma, J. Muller, V. S. Chaluvadi, M. L. Dustin, T. Hla, O. Elemento, J. E. Chipuk, S. R. Schwab, Lymphatic endothelial S1P promotes mitochondrial function and survival in naive T cells. *Nature* **546**, 158–161 (2017).
62. H. Raghu, C. M. Lepus, Q. Wang, H. H. Wong, N. Lingampalli, F. Oliviero, L. Punzi, N. J. Giori, S. B. Goodman, C. R. Chu, J. B. Sokolove, W. H. Robinson, CCL2/CCR2, but not CCL5/CCR5, mediates monocyte recruitment, inflammation and cartilage destruction in osteoarthritis. *Ann. Rheum. Dis.* **76**, 914–922 (2017).
63. O. Kulkarni, R. D. Pawar, W. Purschke, D. Eulberg, N. Selve, K. Buchner, V. Ninichuk, S. Segerer, V. Vielhauer, S. Klussmann, H.-J. Anders, Spiegelmer inhibition of CCL2/MCP-1 ameliorates lupus nephritis in MRL-(Fas)lpr mice. *J. Am. Soc. Nephrol.* **18**, 2350–2358 (2007).
64. F. Mizoguchi, K. Slowikowski, K. Wei, J. L. Marshall, D. A. Rao, S. K. Chang, H. N. Nguyen, E. H. Noss, J. D. Turner, B. E. Earp, P. E. Blazar, J. Wright, B. P. Simmons, L. T. Donlin, G. D. Kalliolias, S. M. Goodman, V. P. Bykerk, L. B. Ivashkiv, J. A. Lederer, N. Hacohen, P. A. Nigrovic, A. Filer, C. D. Buckley, S. Raychaudhuri, M. B. Brenner, Functionally distinct disease-associated fibroblast subsets in rheumatoid arthritis. *Nat. Commun.* **9**, 789 (2018).
65. D. A. Rao, M. F. Gurish, J. L. Marshall, K. Slowikowski, C. Y. Fonseka, Y. Liu, L. T. Donlin, L. A. Henderson, K. Wei, F. Mizoguchi, N. C. Teslovich, M. E. Weinblatt, E. M. Massarotti, J. S. Coblyn, S. M. Helfgott, Y. C. Lee, D. J. Todd, V. P. Bykerk, S. M. Goodman, A. B. Pernis, L. B. Ivashkiv, E. W. Karlson, P. A. Nigrovic, A. Filer, C. D. Buckley, J. A. Lederer, S. Raychaudhuri, M. B. Brenner, Pathologically expanded peripheral T helper cell subset drives B cells in rheumatoid arthritis. *Nature* **542**, 110–114 (2017).
66. G. H. Tesch, S. Maifert, A. Schwarting, B. J. Rollins, V. R. Kelley, Monocyte chemoattractant protein 1–dependent leukocytic infiltrates are responsible for autoimmune disease in MRL-Fas^{lpr} mice. *J. Exp. Med.* **190**, 1813–1824 (1999).
67. W. Stephenson, L. T. Donlin, A. Butler, C. Rozo, B. Bracken, A. Rashidfarrokhi, S. M. Goodman, L. B. Ivashkiv, V. P. Bykerk, D. E. Orange, R. B. Darnell, H. P. Swerdlow, R. Satija, Single-cell RNA-seq of rheumatoid arthritis synovial tissue using low-cost microfluidic instrumentation. *Nat. Commun.* **9**, 791 (2018).
68. A. E. I. Proudfoot, Is CCR2 the right chemokine receptor to target in rheumatoid arthritis? *Arthritis Rheum.* **58**, 1889–1891 (2008).
69. M. Rafei, J. Hsieh, S. Fortier, M. Y. Li, S. Yuan, E. Birman, K. Forner, M. N. Boivin, K. Doody, M. Tremblay, B. Annabi, J. Galipeau, Mesenchymal stromal cell-derived CCL2 suppresses plasma cell immunoglobulin production via STAT3 inactivation and PAX5 induction. *Blood* **112**, 4991–4998 (2008).
70. N. Che, X. Li, L. Zhang, R. Liu, H. Chen, X. Gao, S. Shi, W. Chen, L. Sun, Impaired B cell inhibition by lupus bone marrow mesenchymal stem cells is caused by reduced CCL2 expression. *J. Immunol.* **193**, 5306–5314 (2014).
71. C. Perez-Shibayama, C. Gil-Cruz, H. W. Cheng, L. Onder, A. Printz, U. Mörbe, M. Novkovic, C. Li, C. Lopez-Macias, M. B. Buechler, S. J. Turley, M. Mack, C. Soneson, M. D. Robinson, E. Scandella, J. Gommerman, B. Ludewig, Fibroblastic reticular cells initiate immune responses in visceral adipose tissues and secure peritoneal immunity. *Sci. Immunol.* **3**, eaar4539 (2018).
72. R. T. Palframan, S. Jung , G. Cheng, W. Weninger, Y. Luo, M. Dorf, D. R. Littman, B. J. Rollins, H. Zweerink, A. Rot, A. H. von Andrian, Inflammatory chemokine transport and presentation in HEV: A remote control mechanism for monocyte recruitment to lymph nodes in inflamed tissues. *J. Exp. Med.* **194**, 1361–1373 (2001).
73. B. Lu, B. J. Rutledge, L. Gu, J. Fiorillo, N. W. Lukacs, S. L. Kunkel, R. North, C. Gerard, B. J. Rollins, Abnormalities in monocyte recruitment and cytokine expression in monocyte chemoattractant protein 1-deficient mice. *J. Exp. Med.* **187**, 601–608 (1998).
74. S. Srinivas, T. Watanabe, C. S. Lin, C. M. William, Y. Tanabe, T. M. Jessell, F. Costantini, Cre reporter strains produced by targeted insertion of EYFP and ECFP into the ROSA26 locus. *BMC Dev. Biol.* **1**, 4 (2001).
75. S. Chyou, F. Benahmed, J. Chen, V. Kumar, S. Tian, M. Lipp, T. T. Lu, Coordinated regulation of lymph node vascular-stromal growth first by $CD11c^+$ cells and then by T and B cells. *J. Immunol.* **187**, 5558–5567 (2011).

Acknowledgments: We thank S. Chen-Kiang and C. Blobel for insightful discussions; J. Finik for statistical consultation; E. Pamer for CCL2-GFP, CCR2-GFP, and CCR2-DTR mice; C. Lowell for *Ccl19*-Cre breeders; and J. Cyster and the Lu laboratory for critical reading of the manuscript. Ccl19-Cre [Tg(Ccl19-cre)489Biat] mice are available from Burkhard Ludewig under a material transfer agreement with the Kantonsspital St. Gallen, Institute of Immunobiology. B.J.M. has grant funding from Atyr Corp. and Puretech Corp. and serves as an advisor for Puretech. **Funding:** Supported by MSTP T32GM007739 to the Weill Cornell/Rockefeller/Sloan-Kettering Tri-Institutional MD-PhD Program (W.D.S.), T32AR071302 to the Hospital for Special Surgery Research Institute Rheumatology Training Program (W.D.S.), National Health and Medical Research Council (Australia) Fellowship 1060675 (D.T.), NIH/NCI Cancer Center Support Grant P30 CA008748 (B.J.M.), NIH R01AI079178 (T.T.L.), Alliance for Lupus Research (T.T.L.), St. Giles Foundation (T.T.L.), Scleroderma Foundation (T.T.L.), O'Neill Foundation from Barbara Volcker Center for Women and Rheumatic Diseases (T.T.L.), and NIH Office of the Director grant S10OD019986 to Hospital for Special Surgery. **Author contributions:** D.C.D., H.J.P., C.L.L., W.D.S., S.C., and V.K. designed, performed, and interpreted experiments. D.T., B.L., and B.J.M. contributed to manuscript development. T.T.L. designed, supervised, and interpreted experiments. D.C.D. and T.T.L. wrote the paper. **Competing interests:** The authors declare that they have no competing interests. **Data and materials availability:** All other data needed to evaluate the conclusions in the paper are present in the paper or the Supplementary Materials.

Submitted 15 November 2018
Resubmitted 26 November 2019
Accepted 11 February 2020
Published 20 March 2020
10.1126/sciimmunol.aaw0693

Citation: D. C. Dasoveanu, H. J. Park, C. L. Ly, W. D. Shipman, S. Chyou, V. Kumar, D. Tarlinton, B. Ludewig, B. J. Mehrara, T. T. Lu, Lymph node stromal CCL2 limits antibody responses. *Sci. Immunol.* **5**, eaaw0693 (2020).

Science Immunology

Lymph node stromal CCL2 limits antibody responses

Dragos C. Dasoveanu, Hyeung Ju Park, Catherine L. Ly, William D. Shipman, Susan Chyou, Varsha Kumar, David Tarlinton, Burkhard Ludewig, Babak J. Mehrara and Theresa T. Lu

Sci. Immunol. **5**, eaaw0693.
DOI: 10.1126/sciimmunol.aaw0693

Sending messages to plasma cells

Lymph node stromal cells serve as a platform that facilitates functional interactions between distinct immune cell types. Here, Dasoveanu *et al*. have examined the role of fibroblastic reticular cells (FRCs), a type of lymph node stromal cells, in regulating the survival of antibody-producing plasma cells. They report FRCs to be a critical source of chemokine ligand 2 (CCL2), and that CCL2 produced by FRCs tempers the expansion of plasma cells. Plasma cells do not express the CCL2 receptor CCR2; rather, CCR2-expressing monocytes respond to CCL2 by generating molecules that relay signals from the FRCs to the plasma cells. The study adds to the growing appreciation of the roles of lymph node stromal cells in fine-tuning adaptive immune responses.

Science Immunology (ISSN 2470-9468) is published by the American Association for the Advancement of Science, 1200 New York Avenue NW, Washington, DC 20005. The title *Science Immunology* is a registered trademark of AAAS.

Science Immunology
AAAS

immunology.sciencemag.org/cgi/content/full/5/45/eaaw0693/DC1

Supplementary Materials for

Lymph node stromal CCL2 limits antibody responses

Dragos C. Dasoveanu, Hyeung Ju Park, Catherine L. Ly, William D. Shipman, Susan Chyou, Varsha Kumar, David Tarlinton, Burkhard Ludewig, Babak J. Mehrara, Theresa T. Lu*

*Corresponding author. Email: lut@hss.edu

Published 20 March 2020, *Sci. Immunol.* **5**, eaaw0693 (2020)
DOI: 10.1126/sciimmunol.aaw0693

The PDF file includes:

Other Supplementary Material for this manuscript includes the following:

(available at immunology.sciencemag.org/cgi/content/full/5/45/eaaw0693/DC1)

Data file S1 (Microsoft Excel format).

Figure S1

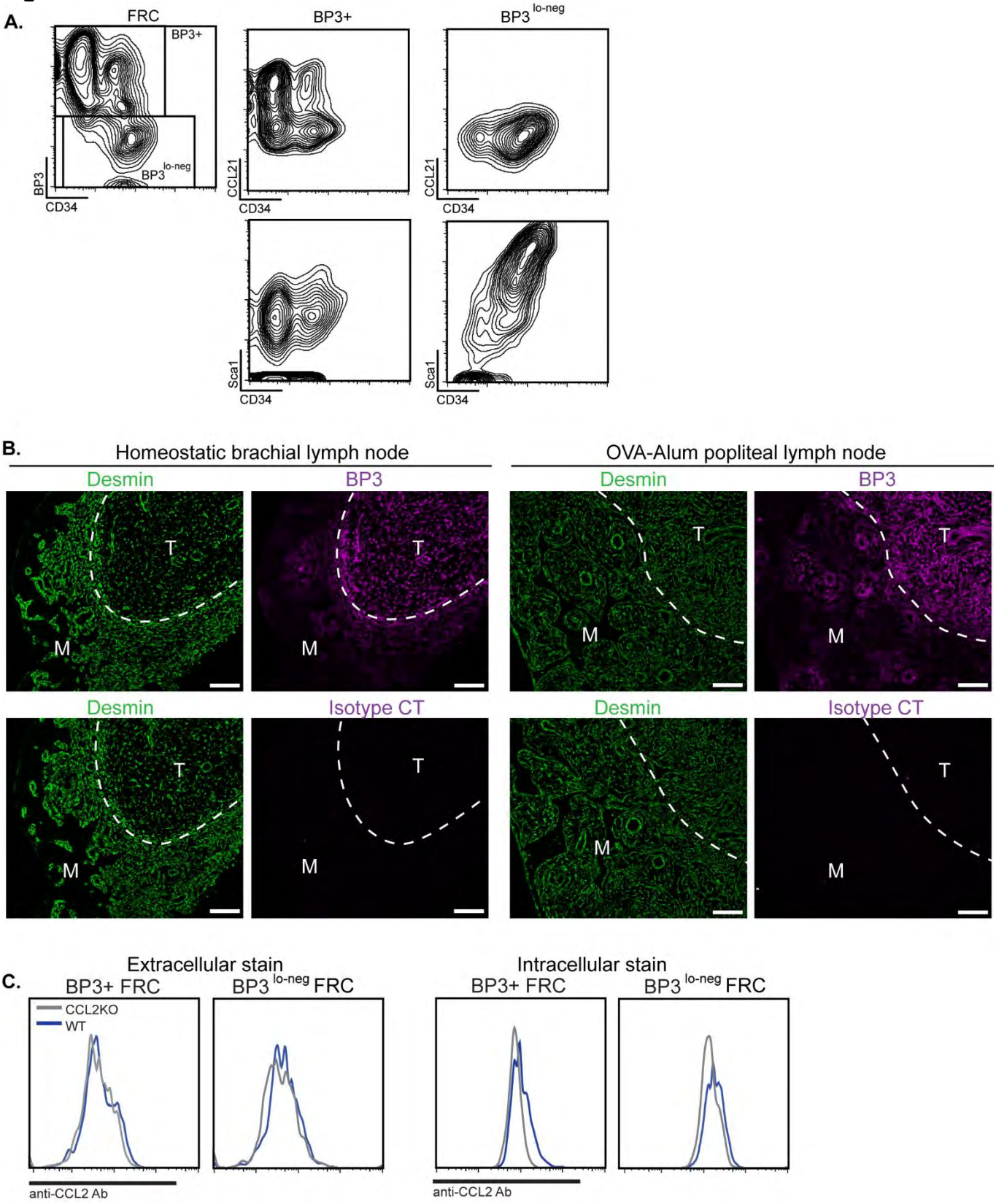
A.
FRC
BP3+
BP3 lo-neg
BP3
CD34
BP3+
CCL21
CD34
BP3 lo-neg
CCL21
CD34
Sca1
CD34
Sca1
CD34
B.
Homeostatic brachial lymph node
OVA-Alum popliteal lymph node
Desmin
BP3
Desmin
BP3
Desmin
Isotype CT
Desmin
Isotype CT
T
M
C.
Extracellular stain
Intracellular stain
BP3+ FRC
BP3 lo-neg FRC
BP3+ FRC
BP3 lo-neg FRC
CCL2KO
WT
anti-CCL2 Ab
anti-CCL2 Ab

Fig. S1. Characterization of BP3^{+} and BP3$^{lo\text{-}neg}$ FRCs. (A) Representative flow cytometry plots showing characteristics of BP3+ and BP3$^{lo\text{-}neg}$ FRCs from homeostatic brachial lymph nodes. **(B)** BP3 staining pattern in T zone and medulla. Sections of homeostatic WT brachial and day 15 WT OVA-Alum immunized popliteal lymph nodes stained for the indicated markers. (M) medulla, (T) T zone. Scale bar is 100 μm. **(C)** Representative histograms showing extracellular and intracellular CCL2 antibody staining of BP3+ and BP3$^{lo\text{-}neg}$ FRCs in homeostatic brachial lymph nodes. **(A,C)** Fluorescence scale is $\log_{10}$.

Figure S2

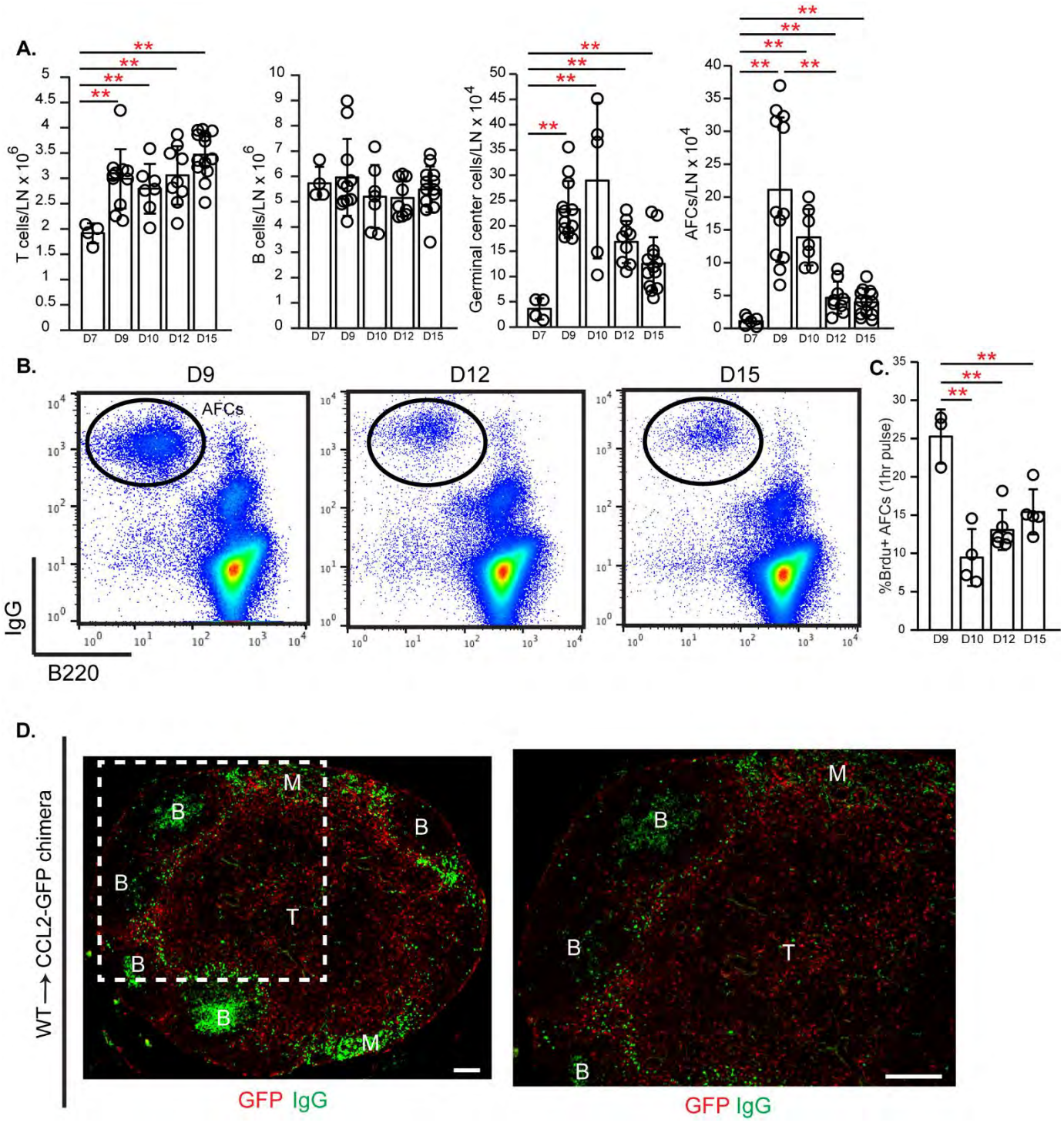

Fig. S2. Characterization of lymph node AFC responses and localization after OVA-Alum. (A-C) WT mice were immunized in the footpad with OVA-Alum and popliteal lymph nodes were harvested at indicated time points. **(A)** Numbers of the indicated cell populations. **(B)** Representative flow cytometry plots showing AFC gating. **(C)** AFC proliferation rate as indicated by percent of AFCs that

are Brdu+. Mice were injected IP with 2 mg Brdu 1 hour prior to euthanasia. **(D)** Lymph node section from WT→CCL2-GFP chimera at day 10 after OVA-Alum immunization, stained for GFP and IgG. Scale bar is 100 μm. Sections are representative of at least 3 mice per condition. **(A,C)** Each symbol represents one mouse; n=3-13 per condition. $^{**}P < 0.01$ using 2-tailed unpaired Student's *t* test. Error bars represent SD.

Figure S3

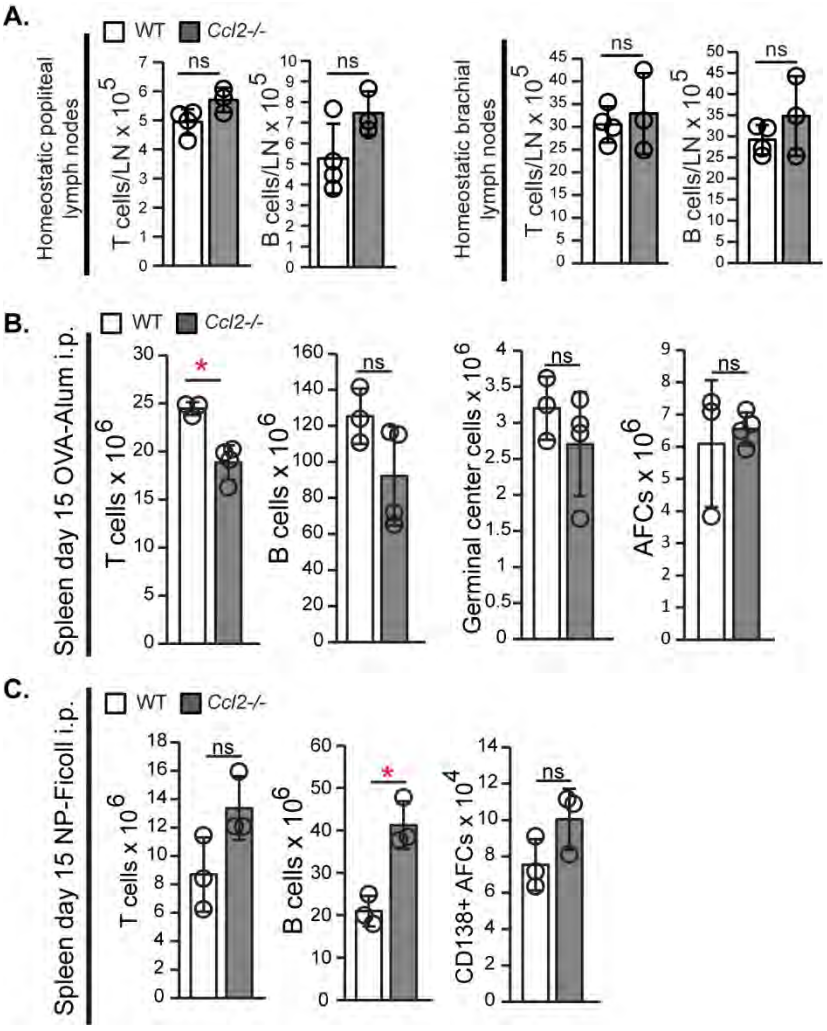

Fig. S3. Characterization of immune cell populations in homeostatic and immunized *Ccl2*$^{-/-}$ lymph nodes and spleens. (A) Numbers of lymphocytes in WT and *Ccl2*$^{-/-}$ homeostatic popliteal and brachial lymph nodes. **(B-C)** Numbers of indicated cell populations in WT and *Ccl2*$^{-/-}$ spleens 15 days after i.p. immunization with OVA-Alum **(B)** and NP-Ficoll **(C)**. **(A-C)** Each symbol represents one mouse; n=3-4 mice per condition. *$P < 0.05$, ns=not significant, using 2-tailed unpaired Student's *t* test. Error bars represent SD.

Figure S4

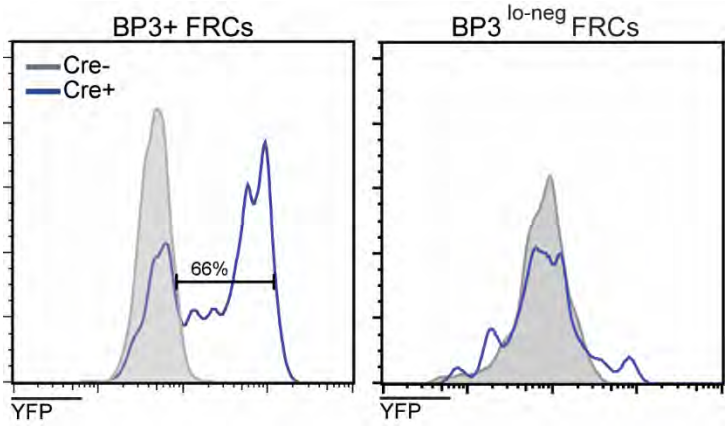

Fig. S4. YFP expression in *Ccl19*-Cre;YFP$^{f/STOP/f}$ FRCs at day 15 after OVA-Alum. Representative histograms showing YFP levels in BP3+ and BP3^{lo-neg} FRCs from *Ccl19*-Cre;YFP$^{f/STOP/f}$ and control YFP$^{f/STOP/f}$ mice. Fluorescence scale is log_{10}.

Figure S5

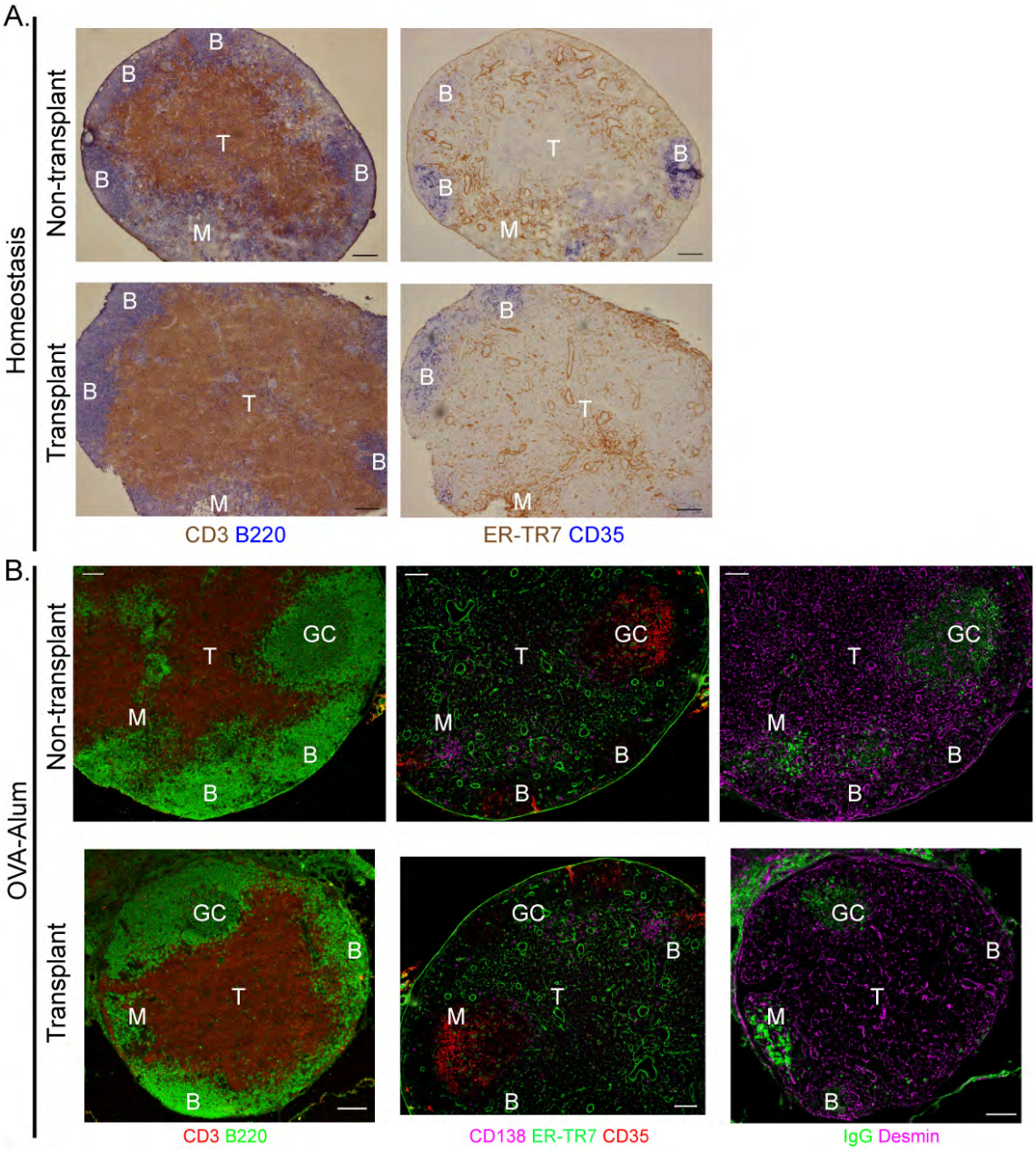

Fig. S5. Transplanted lymph nodes show normal organization. (A) Sections of homeostatic non-transplanted and transplanted popliteal lymph nodes 4 weeks post-transplant stained for the indicated markers. (B) B cell follicles, (T) T zone, and (M) medulla. **(B)** Immunofluorescence staining of D12 OVA-Alum non-transplanted and transplanted popliteal lymph node immunized two months after surgery, stained for the indicated markers. (GC) germinal center, (T) T zone, and (M) medulla. **(A,B)** Scale bars are 100 μm.

Figure S6.

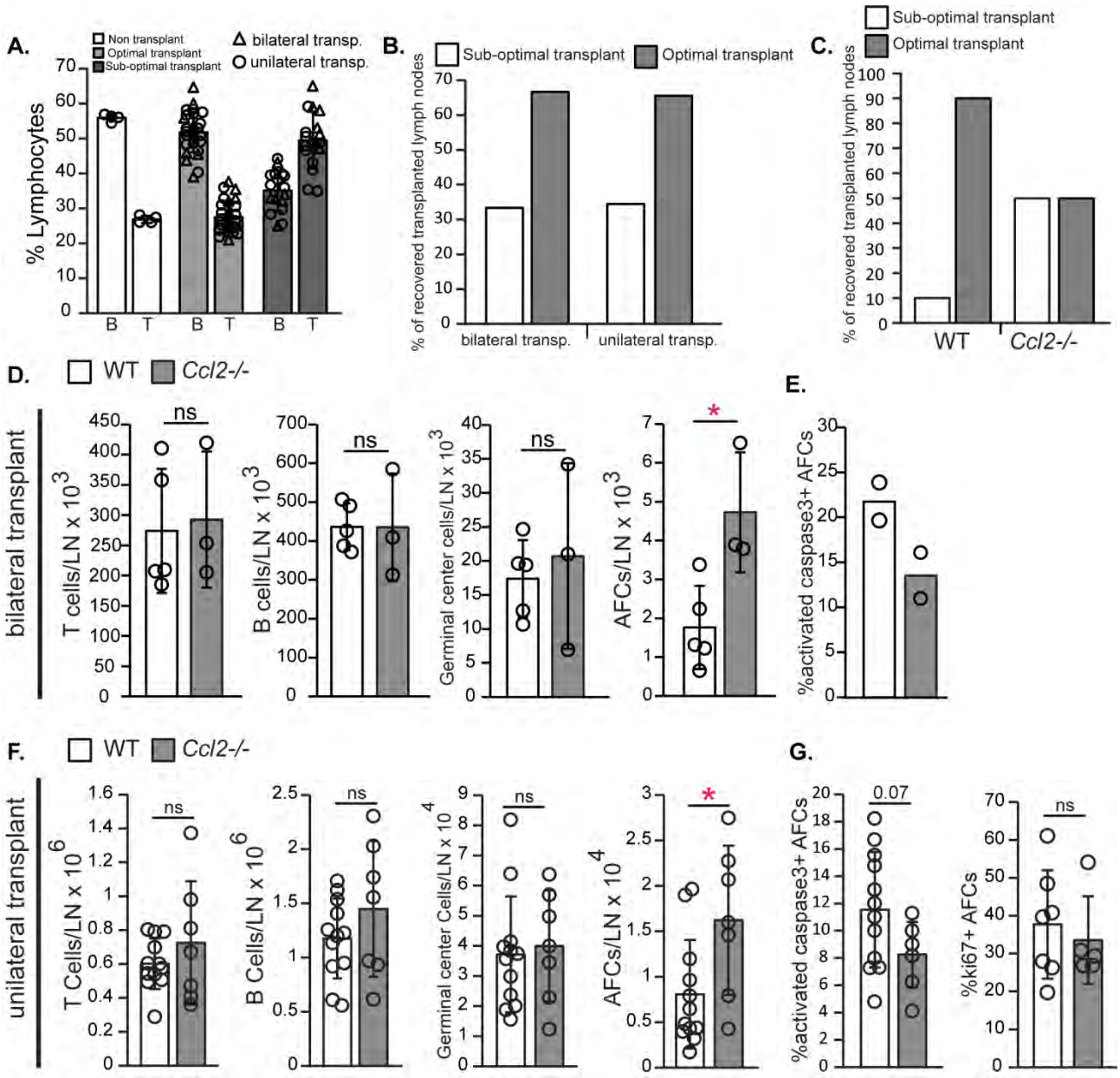

Fig. S6. Analysis of optimal transplants and immune responses. (A-G) 8 to 10 weeks after lymph node transplantations, mice were immunized in the foot with OVA-Alum on the side of the surgery, and the lymph nodes were harvested 15 days later. **(A)** Percent of T and B cells in indicated mouse transplant conditions. **(B,C)** Percent of indicated transplant outcomes in bilateral or unilateral transplant surgeries and WT and *Ccl2*$^{-/-}$ mice. **(D,F)** Numbers of indicated cell populations in bilateral **(D)** and unilateral **(F)** transplants. **(E,G)** Percentage of AFCs that are activated caspase-3+ **(E,G)** and ki67+ **(G)** in bilateral **(E)** and unilateral **(G)** transplanted immunized popliteal lymph nodes

respectively. **(A, D,E,F,G)** Each symbol represents one lymph node; n=3-29 lymph nodes per condition. *$P < 0.05$, ns=not significant using 2-tailed unpaired Student's *t* test. Error bars represent SD.

Figure S7.

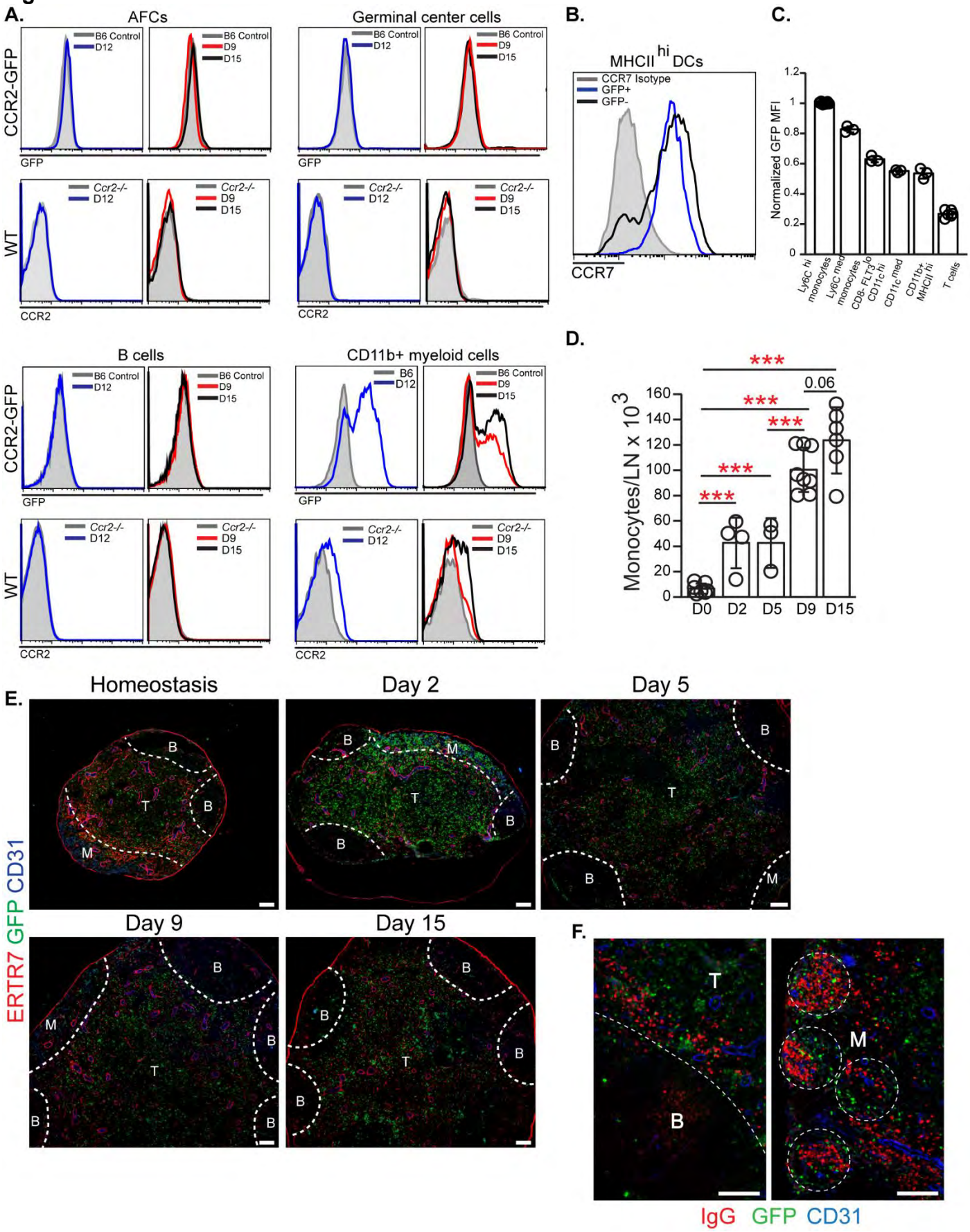
A.
AFCs
Germinal center cells
B cells
CD11b+ myeloid cells
CCR2-GFP
WT
GFP
CCR2
B6 Control
D12
D9
D15
Ccr2-/-
B6
B.
MHCII hi DCs
CCR7 Isotype
GFP+
GFP-
CCR7
C.
Normalized GFP MFI
Ly6C hi monocytes
Ly6C med monocytes
CD8- FLT3lo CD11c hi
CD11c med
CD11b+ MHCII hi
T cells
D.
Monocytes/LN x 10^3
***
0.06
D0
D2
D5
D9
D15
E.
Homeostasis
Day 2
Day 5
Day 9
Day 15
ERTR7 GFP CD31
B
T
M
F.
IgG GFP CD31

Fig. S7. Further characterization of CCR2 expression and CCR2^{+} cell identity, numbers, and localization after immunization. (A) Representative histograms showing CCR2 expression in AFCs, germinal center cells, total B cells, and CD11b+ myeloid cells at days 9, 12 and 15 post OVA-Alum immunization. CCR2 expression was indicated by GFP levels in *Ccr2*-GFP reporter mice and CCR2 antibody staining in WT mice. **(B)** Representative histogram showing levels of CCR7 in CCR2+ and CCR2- MHCII^{hi} DCs. **(C)** GFP MFI in the indicated cell populations of *Ccr2*-GFP mice, normalized to the MFI in Ly6C^{hi} monocytes at day 12 after OVA-Alum immunization. **(D)** Numbers of Ly6C^{hi} monocytes in immunized popliteal lymph nodes at the indicated times post OVA-Alum. **(E-F)** *Ccr2*-GFP mice were analyzed at the indicated time points **(E)** and day 12 **(F)** after OVA-Alum immunization, and popliteal lymph node sections were stained with the indicated markers. Scale bar is 100 μm. Each symbol represents one mouse; n=3-7 mice per condition. $^{**}P < 0.01$, using 2-tailed unpaired Student's *t* test. Error bars represent SD.

Figure S8.

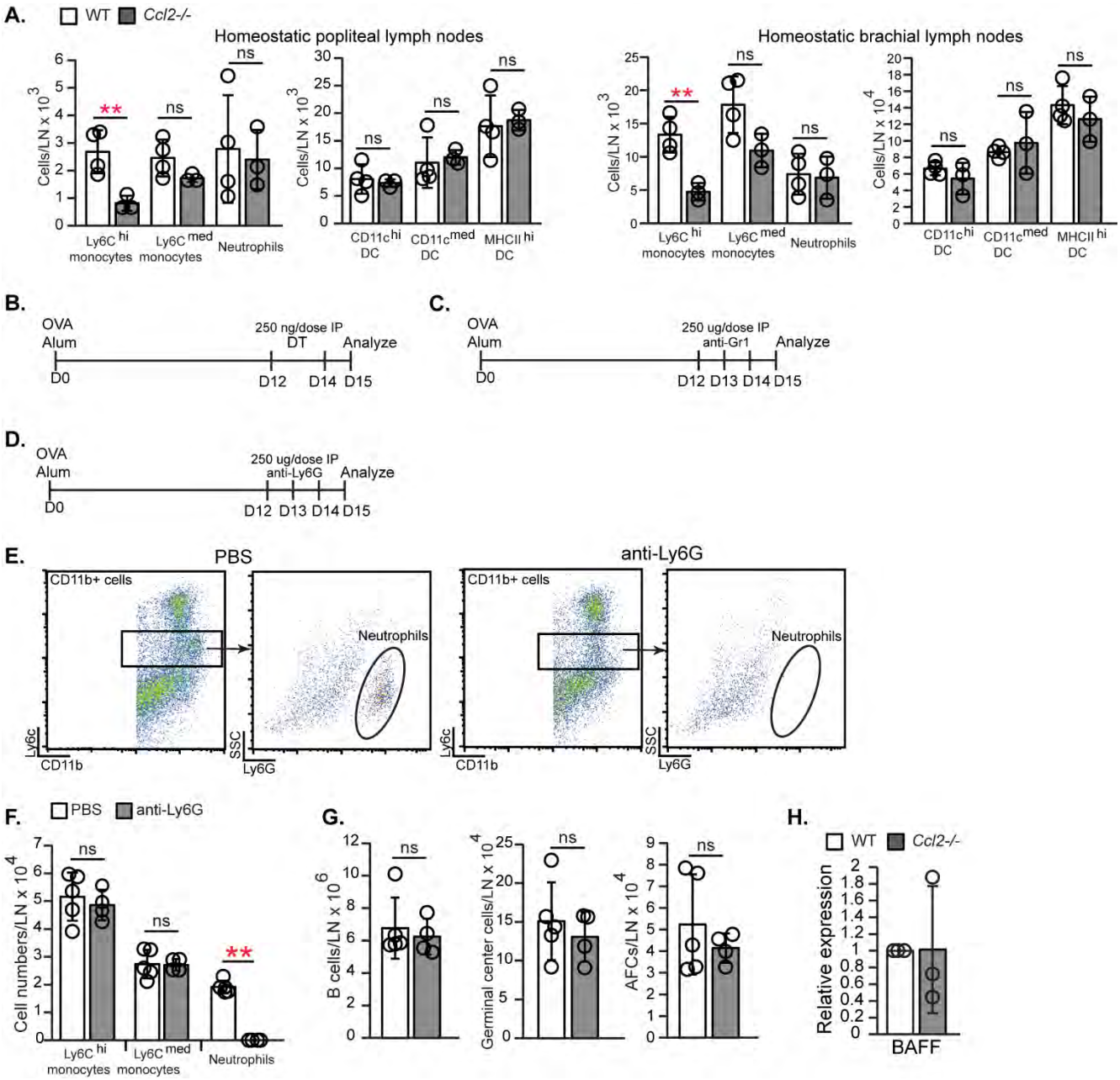

Fig. S8. Monocyte numbers are lower in homeostatic *Ccl2*$^{-/-}$ lymph nodes, and neutrophils do not play a role in limiting antibody responses. (A) Myeloid cell numbers in homeostatic popliteal and brachial lymph nodes of WT and *Ccl2*$^{-/-}$ mice. **(B-C)** IP administration regimen for DT in *Ccr2*-DTR mice **(B)** and anti-Gr1 in WT mice **(C)**. **(D-G)** Anti-Ly6G was administered as shown in **(D)**. **(E)** Representative flow cytometry plots showing neutrophil depletion. **(F)** Numbers of Ly6C^{hi} and Ly6C^{med} (and Ly6G^{neg}) monocytes and (Ly6C^{med}Ly6G+) neutrophils per lymph node. **(G)** Numbers of B cells, germinal center cells, and AFCs. **(H)** Relative BAFF mRNA expression in FRCs from day 15

OVA-Alum immunized lymph nodes. **(A,F,G)** Each symbol represents one mouse **(A,F,G)** and one independent sort **(H);** n=3-5 mice per condition **(A,F,G)** and 7 per sort **(H)**. $^{**}P < 0.01$, ns=not significant using 2-tailed unpaired Student's *t* test. Error bars represent SD.

Figure S9.

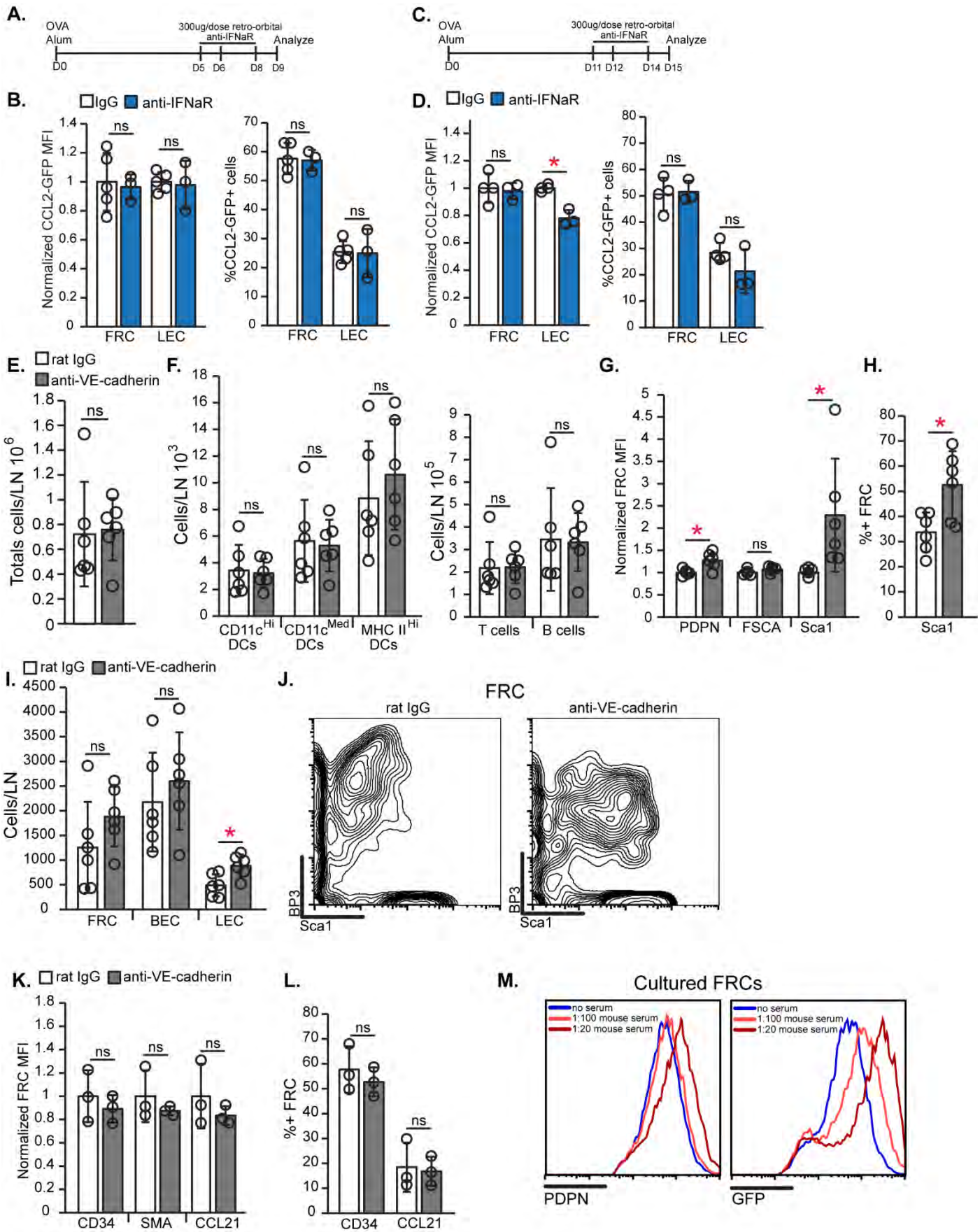
A.
OVA
Alum
300ug/dose retro-orbital
anti-IFNaR
Analyze
D0
D5 D6 D8 D9
C.
OVA
Alum
300ug/dose retro-orbital
anti-IFNaR
Analyze
D0
D11 D12 D14 D15
B.
IgG anti-IFNaR
Normalized CCL2-GFP MFI
%CCL2-GFP+ cells
FRC LEC
D.
IgG anti-IFNaR
Normalized CCL2-GFP MFI
%CCL2-GFP+ cells
FRC LEC
E.
rat IgG
anti-VE-cadherin
Totals cells/LN 10^6
F.
Cells/LN 10^3
CD11c^Hi DCs
CD11c^Med DCs
MHC II^Hi DCs
Cells/LN 10^5
T cells
B cells
G.
Normalized FRC MFI
PDPN
FSCA
Sca1
H.
%+ FRC
Sca1
I.
rat IgG
anti-VE-cadherin
Cells/LN
FRC
BEC
LEC
J.
FRC
rat IgG
anti-VE-cadherin
BP3
Sca1
K.
rat IgG
anti-VE-cadherin
Normalized FRC MFI
CD34
SMA
CCL21
L.
%+ FRC
CD34
CCL21
M.
Cultured FRCs
no serum
1:100 mouse serum
1:20 mouse serum
PDPN
GFP

Fig. S9. Effects of interferon receptor blockade on stromal CCL2, anti–VE-cadherin on cell populations and FRC phenotype, and serum on FRC CCL2. (A-D) CCL2-GFP mice were immunized in footpads with OVA-Alum at Day 0 and injected retro-orbitally with 3 doses of anti-IFNαR or control IgG (300ug/injection) between days 5-8 **(A)** or days 11-14 **(C)**. **(B,D)** FRC and LEC GFP MFIs in anti-IFNαR-treated mice normalized to that in IgG controls (left) and percent of FRCs and LECs that are GFP+ (right)**. (E-L)** Homeostatic mice were injected with 25 ug of anti-VE-cadherin or control IgG in the hind footpads and popliteal lymph nodes were harvested 24 hours later. **(E,F,I)** Numbers of indicated cell populations. **(G,K)** FRC MFIs for indicated markers in anti-VE-cadherin mice normalized to that of IgG control mice. **(H,L)** Percentage of FRCs positive for indicated markers**. (J)** Representative FACS plot of FRCs from control or anti-VE-cadherin treated lymph nodes. **(M)** Histograms showing the levels of the indicated markers in cultured FRCs incubated with mouse serum. Representative of three different FRC cultures. **(B,D,E-I,K,L)** Each symbol represents one mouse; n=3-6 per condition. *$P < 0.05$, ns=not significant , using 2-tailed unpaired Student's *t* test. Error bars represent SD.